EVAPORATED AND RECRYSTALLIZED CdS LAYERS

Technical Report #11
July 27, 1966
NONR (G) 4336 (00)

by
K. W. Böer
Principal Investigator
Physics Department
University of Delaware
Newark, Delaware

SEP 7 1966

A

EVAPORATED AND RECRYSTALLIZED CdS LAYERS[+]

By

K. W. Böer [*]
A. S. Esbitt
W. M. Kaufman

[*]Physics Department
University of Delaware
Newark, Delaware

Applied Research Laboratory
General Instrument Corporation
Newark, New Jersey

ABSTRACT

Heat treatments of evaporated CdS layers in nitrogen containing HCl and traces of oxygen, and providing a transport of CdS and copper are reported. Recrystallization of areas up to several mm^2 are observed. At $25°C$, the treated layers show mobilities of 140 to 230 cm^2 /Vs, photoconductivities of 10^{-3} to $2 \times 10^{-1} \Omega^{-1} cm^{-1}$ at 750 ft-c ($2600°K$ white light) with light-to-dark-current ratios of $10^8 - 10^9$ and response time (decay) of $300 \mu s$ to 1.2 ms at 100 ft-c. The level distribution and capture cross section for electrons is investigated using spectral distribution, light intensity, and temperature dependence of photoconductivity, thermally stimulated current and response time analyses. Levels at 0.23, 0.43, 0.67, 1.05 and 2.05 eV are observed and the letter three attributed to Cu-centers. Compared to other layers and single crystals, these layers show a density of $< 10^{12}$ cm^{-3} of levels attributed to sulfur vacancies in the range between 0.3 and 0.65 eV and a not detectable amount of intrinsic defects acting as quenching centers at 0.9 and 1.35 eV. This is explained by a Cu-enhanced recrystallization in a CdS-supplying atmosphere at temperatures ($620°$ to $650°C$) below the temperatures otherwise used for crystal growth, and thereby efficient annealing of intrinsic defects.

1. INTRODUCTION

The evaporation of photoconducting compounds in vacuum as a method for layer deposition has been known for a long time as a relatively simple and reproducible way to obtain photoconducting films. It yields better defined layers of higher purity and allows better doping than other methods of layer deposition as e.g., chemical decomposition, powder spraying and sintering.

However, directly after deposition, evaporated layers show very poor photoelectric properties, as low carrier mobilities, low photocurrent-to-dark-current ratio (hereafter called L/D) and time response to rapid changes in illumination level, which all are far inferior to those of good photoconducting single crystals.

A reason for this is that the vacuum deposition onto a relatively cold substrate is a non-equilibrium process and yields to highly disordered layers of nonstoichiometric composition. In CdS with a large mass ratio of the components a layer with considerable excess of the heavier component (Cd) must be expected, since from the phase diagram (minimum vapor pressure lies in the cadmium rich region) no compensation of the mechanical effect of predominant desorption of the lighter component can be expected. A rise of the substrate temperature during evaporation shifts the composition of the layer favorably, and the enhanced surface diffusion during growth reduces the density of intrinsic defects. However, the attainable evaporation rates from baffled sources (see paragraph 2) limit the substrate temperature to

about 200°C, a temperature still too small to yield layers of desired close-to-stoichiometric composition. On the other hand, with higher temperatures it becomes increasingly difficult to maintain substrate temperature and evaporation rate so that the growing velocity of the layers stays small enough to permit improved crystalline growth.

It therefore seems necessary to submit the vacuum deposited layers to further treatment. Various post-deposition treatments have been reported, as e.g. heat treatment in vacuum,[1-3] or in different gas atmospheres, for example, argon, nitrogen, oxygen, and cadmium vapor[2,4,5,25] and utilization of a Cu or Ag enhanced recrystallization.[6-9] By some of these methods one is able to increase grain size and improve crystal boundary properties to the extent that effective mobilitess approach values observed in single crystals. However, the photoelectric properties are still inferior to those of single crystals or otherwise deposited layers. Table 1 summarizes some results of post-deposition treatment as described in the literature.

Author	Photoconductivity at intensity	L/D ratio at intensity	Rise and decay time at intensity	Mobility at 25°C
Sakai and Okimura	$5 \times 10^{-2} \Omega^{-1} cm^{-1}$ at 100 ft-c	10^4 at 100ft-c	0.15 and 0.02s at 10 ft-c	
Lakshamanan and Mitchell	$2 \times 10^{-5} \Omega^{-1} cm^{-1}$ at 1000 ft-c	10^3 at 1000 ft-c	3 ms and 6 ms at 500 ft-c	
Dressner and Shallcross	$0.2 \, \Omega^{-1} cm^{-1}$ at 1 Watt/cm^2	$10^6 \ldots 10^8$ at 1 Watt/cm2		up to 180 cm²

Table 1

Dressner and Shallcross' investigations also indicated that in addition to allowing for recrystallization, the post-deposition treatment should provide conditions for epitaxial growth, while maintaining a desired nearly stoichiometric composition.

This paper describes a new method for treating evaporated CdS films which leads to recrystallized layers with mobilities above $200 cm^2/Vs$ and unusual low density of intrinsic defects resulting in markedly improved photoconductive properties compared with the values reported above. The level distribution of these layers is investigated and discussed.

2. EVAPORATION OF CdS LAYERS

The CdS films were evaporated at a pressure of 10^{-5} torr from a tungsten evaporant source.[a] General Electric electronic grade CdS powder #118-8-2 was used. All layers were deposited onto 1/16" thick soda-lime glass slides. The slides were cleaned before being placed in the vacuum system in a sequence consisting of the following steps: one minute immersion in an ultrasonically agitiated solution of Alconox detergent, followed by a deionized water rinse; immersion in Chromerge at 180°C for 5 minutes, followed by a deionized water rinse and immediate drying in a strong stream of purified nitrogen. The slides were then placed in the vacuum chamber and exposed to a 20minute 2500 volt ac glow discharge in argon at 1.5 torr. They were then baked at

----

[a]The design of the source (Mathis Co., Model SM-10) provides for baffling which prohibits powder particles from following a direct path to the substrate, thereby essentially eliminating pinhole formation.

300°C for 20 minutes at 10^{-5} torr. After reducing the substrate
temperature to 180°C, the CdS was evaporated. During the initial
2 minutes of evaporation a shutter was used to shield the substrate
from the charge; the evaporation was continued for 20 minutes.
The CdS films were pin-hole free and did not peel from the sub-
strate during the following heat treatment. The thickness of the
layers was 1 μm $\pm$ 10% and was determined by the interference
method and by weighing.

3. METHODS OF MEASUREMENT

For current measurements, electrodes were provided by
placing two circular indium discs (each 3.8 mm in diameter and,
if not otherwise stated, separated by 0.8 mm) on the surface[b]
and holding them in place with spring loaded wires. For photo-
current measurements, described in paragraph 4, the layers were
illuminated at 730 ft-c with white light (if not otherwise
stated, unfiltered, tungsten source, color temperature 2600°K).
Dark current measurements were made about 30 seconds after removal
of illumination. The applied voltage was 45 volts dc. Currents
were measured with a Hewlett-Packard Microammeter Model No. 425.

The photocurrent measurements described in paragraph 5
were done using a tungsten source (color temperature 2600°K)

----

[b]Punched out indium discs were used with their raised edges
facing downward resulting in good contacts at their circum-
ferences, thus, eliminating major shadow areas between the
electrodes.

in conjunction with a set of Wratten calibrated neutral density filters, and additional filters, as described in the figure captions. The tungsten source was also used in conjunction with a Bausch and Lomb grating monochromator #33-86-25 using slit widths of 1.35/0.75 mm, and usually[c] with Corning glass filters in order to suppress higher order interference regions. The optical assorption of the layers was observed with a Perkin-Elmer 1326 spectrometer. The current through the layer was measured with Keithley linear or logarithmic micromicroammeters Model 413A, 412, or 415. Applied voltages between 1.5 and 12 volts were chosen (if not otherwise stated, 10 volts was used).

Long-time rise and decay measurements of the photocurrent as well as TSC curves were recorded on a Houston Hr-96 x-y recorder, using a time display on the x-axis. Fast response time measurements were done using a Tektronix 543A oscilloscope with type L plug-in preamplifier; the load resistor in the photoconductor curcuit was variable and chosen so that the displayed signal never exceeded 5% of the voltage applied to the layer. A fast acting mechanical shutter was used for switching the light (half-time for opening or closing $\leq$ 120μs).

For the measurements described in paragraph 4 and for the Hall effect the layers were exposed to air ambient, for those

----

[c]These filters were omitted in the visible range since a small amount of additional UV has no marked influence on the photocurrent.

in paragraph 5 the layers were kept at 10^{-3} torr in a stainless
steel vacuum vessel with glass windows. Heating and cooling
of the CdS layer was accomplished by means of a cooling finger.
For fast temperature equalization the layer was held in the center
of a copper cavity having small holes to permit optical excitation.

The Hall effect was measured at 5k Gauss using a Varian
electromagnet with 7 cm spacing. A five electrode method
was employed with evaporated indium electrodes, and the potential
difference was measured with Keithley 600A Electrometers.

4. RECRYSTALLIZATION AND DOPING

The apparatus used for heat treatment of evaporated CdS
layers is shown in Figure 1. CdS coated slides, 16 x 50 mm,
were placed inside a 36 mm ID quartz tube which is partially
filled along its length of 50 cm with a layer of CdS powder.
A layer of 320 mesh copper powder (99.9% pure) was spread onto
the CdS powder as an effective means for copper-doping the films
and enhancing recrystallization during the heat treatment.
The slides were placed close together on the powder with the
CdS evaporated layer facing upwards. The tube was then inserted
into the furnace which was at the desired treatment temperature.

Two ovens were used in series in order to heat the powder
at the inlet end of the tube to a slightly higher temperature
than that maintained in the remainder of the tube. Gas inlet
and outlet fixtures were provided and a gas mixtrue was contin-
uously flowing over the slides during the heat treatment. The
mixture consisted of selected percentages of oxygen and HCl in
nitrogen carrier gas with the total flow kept constant at 3600 cm^3/min. The

oxygen (99.6% purity) and nitrogen (99.996% purity) were taken from supplier's tanks and their relative flow rates measured with calibrated flowmeters. HCl was provided by bubbling part of the oxygen-nitrogen mixture through a wash bottle containing a measured amount of 37% aqueous HCl.[d] The "HCl flow rate" is defined as the ratio of the flow through arm (1) to that through arm (2) in Figure 1. The heat treatment was performed for 30 minutes, after which the oxygen and HCl flow were turned off and the ovens were allowed to cool under nitrogen flow alone. When cooled below 150°C the treatment tube was removed from the oven. Further cooling to room temperature was then continued in room ambient.

Figure 2 shows the photo- and dark-currents of treated CdS layers as a function of their position in the furnace, together with the temperature profile along the tube. It is seen that with increasing treatment temperatures above 300°C the light and dark conductivities increase by orders of magnitude and at still higher treatment temperatures up to 600°C they decrease; however, the L/D ratio stays below ten in this region. At temperatures greater than 600°C, the dark conductivity remains low but the photoconductivity increases rapidly resulting in

----

[d] 30 cm³ in a 48 mm ID wash bottle having a 5 mm ID tube ending 10 mm below the surface of the acid. The HCl enriched part of the carrier gas is then dried using a drying tube filled with $CaCl_2$.

a high L/D ratio. The maximum photocurrent and L/D ratio occurs between 620°C and 650°C and the layers were therefore treated within this temperature range in the experiments reported below.

Figure 3 shows the photo- and dark-current as a function of the HC1 flow rate. The current values plotted are the average values for at least 8 samples treated at the particular rate. The mean variation among such samples was less than one order of magnitude. A nitrogen-oxygen mixture of 0.25 volume percent oxygen was used and 15 grams of copper powder was spread on the CdS powder layer. The curve shows a broad maximum peaking at 7% HC1 flow rate with an L/D ratio of about 10^8.

Figure 4 shows the effects of varying the composition of the oxygen-nitrogen mixture. The curves labelled "a" give the photo- and dark-currents for treatments performed at a 7% HC1 flow rate and 15 g of spread copper. When no HC1 or copper is provided, the "b" curves are obtained which indicate a photo-sensitivity orders of magnitude lower. The highest photosensi-tivity is observed at 0.25% oxygen which is the value used for the treatments described in Figure 3. For both sets of curves treatments with 10% or more of oxygen resulted in a substantial loss of the layers (see also[10]).

In Figure 5, the photo- and dark-current variations with the amount of spread copper is shown. There is a maximum in photo-sensitivity at 15 g copper (the value used in Figure 3 and for curves "a" of Figure 4). At higher copper concentrations a con-ducting layer, black to brown in color, is deposited on top of

the CdS films, thereby decreasing their resistivity, and ruining
their photoconductive properties.

5. PROPERTIES OF OPTIMIZED CdS LAYERS

Films exhibiting the highest photosensitivity were those
heat treated at 620-650°C on a bed of CdS containing 15 g of
copper under a flowing gas mixture containing 0.25% oxygen in
nitrogen with an HCl flow rate of 7%. Their photoconductivity
at 730 ft-c illumination and 25°C lies between 10^{-3} and $0.2 \Omega^{-1}cm^{-1}$,
the L/D ratio between 10^8 and 10^9.

The optical transmission of samples before and after this
treatment is shown in Figure 6. The transmission of treated
films near the absorption edge shows a marked increase in slope.

Visual observation of the layers using polarized light shows
uniform areas up to several mm in diameter. The layers have an
ohmic current-voltage characteristic with pressed-on indium
contacts down to about 50 mV and up to over 100 volts (Figure 7).
With evaporated indium electrodes preventing a shadow area near
the electrodes, the ohmic range extends to below 1mV.

The Hall-mobility was measured at room temperature under
150 ft-c illumination with white unfiltered light for three
layers, giving $\mu(1) = 138$ cm^2/Vs, $\mu(2) = 220$ cm^2/Vs, and
$\mu(3) = 225$ cm^2/Vs. For irradiation at 560 mμ and 460 mμ, layer
No. (3) shows mobilities of 230 cm^2/Vs, and 180 cm^2/Vs, respec-
tively. The side length of the triangle between the potential
electrodes for the Hall-effect was 1 mm for the first two layers
and 2 mm for the third layer.

For the following investigations layer No. (3) was chosen.
This layer shows a slightly lower photoconductivity of about
$2 \times 10^{-3} \Omega^{-1} cm^{-1}$ at 730 ft-c white light[e] and room temperature
but a high L/D ratio and a fast response time.

5.1 STATIONARY MEASUREMENTS

Figure 8 shows the photocurrent vs. reciprocal temperature
for different intensities of white light. These curves are almost
temperature independent at low temperatures, and exhibit an
exponential decrease of the photocurrent with increasing tem-
perature with a slope of 0.35 eV, independent of the light intensity;
they then level off starting at about +40°C. The knee between
the low temperature part and the exponential decrease shifts
exponentially towards lower temperatures with decreasing light
intensity with a slope of about -0.35 eV (dashed line in Figure 8).

In Figure 9 a cross section through the curves of Figure
8 is shown for demonstration of the dependence of the photocurrent
on light intensity at different temperatures between 25° and
-150°C. At lower light intensities there exists a superlinear
range[f] with exponents up to 2, which is shifted toward higher
light intensities with increasing temperatures; thus, at -150°C
superlinearity is found only up to 3×10^{-3} ft-c, while at room

----

[e] filtered as indicated for Figure 8

[f] Some of the curves show a hint of a decrease of slope also at
very low intensities.

temperature it persists up to the highest used light level of 25 ft.-c. Above the superlinear range, a practically linear range is observed which, between -150° and -100°C, extends from 3×10^{-3} to 25 ft-c.

The spectral distribution of the photocurrent at 25°C and at -180°C is given in Figure 10. The arrows adjacent to the measured dots indicate slow (more than 10 s) rise or decay to the given stationary values; at wavelengths longer than 1.2 µ, the time constant increases up to many hours. A broad maximum at 580 mµ (25°C curve) and at 560 mµ (-180°C), and a steep (exponential) decrease of photocurrent toward longer wavelength is observed. At 520 mµ (25°C) and 497 mµ (-180°C) another smaller maximum occurs followed by a steep decrease toward shorter wavelengths. For wavelengths below 480 mµ the photocurrent seems to decrease with decreasing wavelength only because of decreasing light intensity. After correction for equal number of photons/cm^{2}s using a linear law for -180°C and a square law for +25°C as indicated in Figure 10 the solid branches of the curves show no more marked dependence on the wavelength.

In the infrared region the photocurrent at 25°C decreases below 10^{-12} a above 850 mµ, while at -180°C the photoconductivity extends up to 1.7 µ, and shows a pronounced maximum at about 1.2µ.[g]

----

[g]At wavelength larger than 800 mµ a change in light intensity from the monochromator and due to the filter CS 7-57 was corrected using a linear photocurrent vs. intensity law (solid curve).

There is no marked quenching connected with the photocurrent
minimum at 1.05μ, i.e., with photoexcitation in the 500 to
650 mμ range even at very low light levels, and no decrease
in photocurrent with additional 1.05μ irradiation was observed.
Also the well known quenching maxima at 950mμ and at 1.35μ
could not be detected at -180°C and at +25°C.

5.2 NONSTATIONARY MEASUREMENTS

The dependence of the decay time on intensity of white,
unfiltered light is given in Figure 11 for 25°C and -180°C.
At 25°C the decay curve shows an almost intensity-independent
range of about 300μs decay time between 50 and 200 ft-c. The
lowest values obtained at -180°C are 2 ms at 200 ft-c. Figure
12 shows typical rise and decay curves as obtained for 200 ft-c
white light at 25°C and -180°C. Figure 13a, curve (1) shows
in a semilogarithmic normalized plot that at -180°C the photo-
current decays by seven orders of magnitude within less than
5 s and by nine orders of magnitude in less than 100 s, if the
layer was first kept at room temperature under white illumination
(400 ft-c) for several minutes, then cooled to -180°C at which
time the light was shut off. The intensity of pre-irradiation
influences the decay time as can be seen from curves (2) and (3)
in Figure 13a. A further irradiation at low temperatures without
intermittant pre-irradiation at room temperature makes the
photo-decay even slower (see curves (4), (5), (6), and (7)).
The photo-decay after irradiation with infrared light (curves
(8) and (9)) is also slow. Figure 13b shows the temperature

dependence of the photocurrent decay for otherwise the same
pre-irradiation conditions as (1) in 13a.

A typical slow rise curve for low excitation densities
(3.1 x 10^{11} photons/cm^{2}s) at -180°C at 495 mμ is plotted in Figure
14 (curve (1)). A similar behavior is shown in the rise curves
at 750 mμ and 800 mμ for about 500 times higher photon density
(curves (2) and (3)). All these curves exhibit a plateau (not
shown in the figure) ending after about 75 to 250 s. Even at
room temperature a plateau can be observed ending after about
7 s after the start of excitation with 3.7 x 10^{11} photons/cm^{2}s
(curve (4)). At slightly higher temperatures (70°C) this plateau
disappears completely (curve (5)). Here a steep rise to a maximum
is followed by a decrease of almost one order of magnitude
(overshoot of the photocurrent).

Figure 15 shows the dependence of the rise and decay time on
the wavelength of excitation (measured towards shorter wavelengths
and at the lower temperature first). For these measurements the
grating monochromator was used without additional filters, thus
the number of photons/cm^{2}s can be obtained from the lower part
of Figure 10. The increase in rise and decay time below 550 mμ
may be attributed in part to the decrease of photons/cm^{2}s avail-
able for excitation.

The dependence of the decay time on light intensity for
monochromatic light at the band edge (20% absorption point) is
given in Figure 16 for different temperatures.

Figure 17 shows a set of thermally stimulated current
(TSC) curves for different pre-irradiation conditions. It is

remarkable that the height of a TSC curve is changed in an unusual manner depending on pre-irradiation. After excitation at only -180°C, the highest TSC curves with a peak at about -135°C are observed. Additional infrared illumination at 1.0μ reduces these TSC curves somewhat. White irradiation at room temperature preceding the cooling-down reduces the TSC curve markedly, the more so, the higher the intensity of the preceding irradiation. By this procedure the TSC peak can be reduced by four orders of magnitude using white light of 200 ft-c for pre-irradiation. However, independent of the irradiation history, the range between -45° and +20°C always shows an extremely low conductiviey of less than $10^{-11} \Omega^{-1} cm^{-1}$ (the lower part of the measured curve is within the noise level; the noise has not been substracted). At temperatures above 20°C the conductivity increases exponentially with temperature up to 130°C with a uniform slope of 0.67 eV.

6. DISCUSSION

The visual observation of large uniform areas in which the absorption edge is markedly steeper than for CdS-layers re-crystallized _during_ evaporation, as well as the high mobility, and the ohmic current-voltage characteristics down to below 1 mv indicate a high degree of recrystallization in areas with diameters larger than the electrode distance used. The fact that the Hall-mobility lies only 20 to 50% below the mobility observed in "good" single crystals (attributed to photon scattering) indicates that crystallite boundary effects are almost completely eliminated.

It therefore seems appropriate to calculate the conductivity
with the following elementary formula for circular electrodes:

$$\sigma = \frac{I}{\pi V h} \ln \frac{D}{d} \qquad (1)$$

where I is the current, V the applied voltage, h the layer
thickness, D the center to center electrode distance and d the
electrode diameter.

6.1 FERMI LEVEL

From the onset of infrared photoconductivity at $1.7\mu \triangleq 0.73$ eV
(see Figure 10) one concludes the position of the Fermi level
to be at 0.73 eV below the conduction band. A similar result
(0.67 eV) can be obtained from the exponential increase of the
dark conductivity with the temperature above 20°C (see Figure 17).
The agreement between optically and thermally determined positions
of the Fermi level is good, since a shift of this level due
to Franck-Condon principle in the observed direction can be
expected, and it is very difficult to determine the threshold
for infrared photoconductivity because of a long time constant
of the photoconductivity in this range, and, therefore, possible
errors because of stray light.

From the position of the Fermi level one calculates an
electron density

$$n = N_c \exp - \frac{E_c - E_F}{kT} \qquad (2)$$

with $N_c = 2 (m_{eff} kT/2\pi\hbar^2)^{3/2}$ and $m_{eff} = 0.2 m_o$, which, e.g. at
$T = 333°K$ gives $n = 1.6 \times 10^7$ cm^{-3} (see Figure 17). From the
measured current at the same temperature one obtains with
Eq. (1) $\sigma = 6.5 \times 10^{-10} \Omega^{-1} cm^{-1}$. Using the electron concentration

as given from Eq. (2) this results in an electron mobility of $\mu = 250$ cm^2/Vs, which, within the experimental error, agrees with the mobility measured at considerably higher conductivities under homogeneous optical excitation, and indicates temperature independence of the Fermi level* caused by a dense trap level here.

6.2 LEVEL DISTRIBUTION BELOW THE FERMI LEVEL

From the infrared photocurrent maximum at 1.2μ one obtains another group of levels at 1.05 eV. The fact that no quenching is observed indicates that the density of the well known hole traps at 0.95$\mu \hat{=} 1.3$ eV and 1.35$\mu \hat{=} 0.9$ eV is small compared to that of single crystals,** or that there exist other hole traps with much higher capture cross sections for holes. The second possibility is less probable than an explanation since it was not possible to <u>fill</u> these quenching levels with holes by <u>infrared excitation.</u>

From the exponential decrease of photoconductivity with temperature as shown in Figure 8, a level at 0.35 eV above the valence band is indicated, i.e., 2.05 eV below the conduction band. The fact that the slope of the lnI vs. 1/T curve does

---

*A slight shift due to change of the band gap with temperature is probably compensated by a decrease in mobility with increasing temperature.

**For the used IR intensities up to 10^{16} photons/cm^{2}s quenching in CdS single crystals is found to be at least four orders of magnitude above the comparable detection limit in these layers.

not depend markedly on light intensity down to very low intensities
may be interpreted as caused by a very low density of levels
between the Fermi level and the 2.05 eV level, or by the assumption
that this level has a capture cross section for holes which is
large compared to that of all other hole traps. On the basis
of the measured spectral distribution of the photocurrent the
first possibility has to be rejected.

From the long wavelength edge of the photoconductivity
having a knee at 630 mμ $\simeq$ 1.96 eV at 25°C, probably the same
defect center can be recognized. The difference in positions
of 0.09 eV must be attributed to the shift of the level due to
the change in the charge of its center and to the Franck-Condon
principle.

6.3 LEVEL DISTRIBUTION ABOVE THE FERMI LEVEL

From the fact that the slope of the lnI vs. 1/T curve
(Figure 8) is constant over a wide temperature range and inde-
pendent of light intensity one also can conclude that the density
of electron traps in the corresponding range of quasi-Fermi
level for electrons E_{Fn} must be small as compared to the trap
density near the Fermi level E_F.

This can easily be seen if one takes into consideration
that in the thermal quenching range the holes in the valence
band are in equilibrium with the trapped holes in the 2.05 eV
hole trap. The hole density in the valence band, however,
determines the recombination over fast centers and therefore
the measured density of conduction electrons. Since, because of

quasi-neutrality, the hole density in hole traps is about equal
to the density of trapped electrons, one therefore can write
for the range of thermal quenching:

$$n \propto \left(\int_{E_F}^{E_{Fn}} n_t (E) \ dE \ exp - \frac{E_a - E_v}{kT} \right)^{-1} \qquad (3)$$

with n_t (E), the energy density of trapped electrons, E_a the
energy of the hole trap (here 2.05 eV), and E_v the upper edge
of the valence band. Eq. 3 shows immediately that the slope of
the ln n vs. 1/T curve is constant and determined by $E_v - E_a$
only, if the density of trapped electrons does not depend
markedly on light intensity or temperature. This can be fulfilled
only if the trap density in the corresponding range of quasi-
Fermi level is very small as compared to deeper traps near the
Fermi level already filled with electrons.

Therefore one concluded from Figure 8 that in the range
$0.3 < E_{Fn} < 0.6$ eV, for which the slope of the ln I vs. 1/T
curve is constant, the trap density must be small compared with
the density of traps between 0.6 and 0.67 eV.

TSC curves agree with this observation to the extent that
they show a deep valley between $-60^{\circ}C$ and room temperature.
If one assumes thermal equilibrium between trapped electrons and
the conduction band for the TSC curve, one obtains information
about the energy distribution of traps from the position of the
quasi-Fermi level according to

$$E_c - E_t \simeq E_c - E_{Fn} = kT \ ln \ N_c/n$$

The TSC curves of Figute 17 are redrawn using Eq. 2a in Figure 18

and show the deep valley in trap density to lie between 0.66 and 0.3 eV. Figure 18 also shows a pronounced shallow trap level at about 1.23 eV.

Some information about the trap density can be obtained from

$$N_t = \frac{\int I dt}{e \, G V_o} \qquad (4)$$

where V_o is the volume of the layer between the electrodes $\simeq 5 \times 10^{-6} cm^3$, and G is the gain factor:

$$G = \frac{\tau_c}{\tau_D} \qquad (5)$$

with τ_c = lifetime of electrons in the conduction band and τ_D = their drift time from electrode to electrode.

For steady state optical excitation the gain factor can easily be determined.

From

$$\tau_c = \frac{I}{\pi e \mu V \, \xi a_o} \ln \frac{D}{d} \qquad (6)$$

and

$$\tau_D = \frac{l^2}{\mu V} \qquad (6a)$$

where a_o is the photon density $(cm^{-2} s^{-1})$ incident on the layer, ξ is the ratio of absorbed to incident light, μ is the mobility, and l is the distance between cathode and anode. From Figure 10 one obtains the values given in Table 2 at a wavelength at which the absorption can easily be measured and is small enough (20%) to insure an approximately homogeneous excitation (assuming $\mu = 200 \, cm^2/Vs$).

Temp.	Wavelength λ	Photon density	Photocurrent	Electron lifetime	Drift time at 10 Volts	Gain factor
25°C	515 mμ	9×10^{13} photons/cm^{2}s	1.4×10^{-7} a	7 μs	3.5 μs	2
-180°C	495 mμ	3×10^{13}	2×10^{-6} a	140 μs	3.5 μs	40

Table 2

If one assumes the same electron life time for TSC curves as for similar stationary photocurrents this would lead for the TSC peak at -135°C to a gain factor of G (-135°C) $\simeq$ 40 and for the -20°C minimum of the TSC curve to G (-20°C) $\simeq$ 1. The so calculated trap density for the 0.23 eV center is N_t(0.23) $\simeq 10^{16}$cm^{-3} while the density in the miniuum between 0.45 and 0.65 eV is N_t(0.45 - 0.65) $\simeq 10^{13}$cm^{-3}.

However, as will be discussed below, the lifetime of electrons for TSC curves is probably below the value obtained from stationary photoconductivity. Thus the trap density given above is an upper limit.

More detailed information about the electron-trap distribution can be obtained from the temperature and intensity dependence of the decay-time τ_d. The trap density at the position of the quasi-Fermi level, E_{Fn}, and in an energy interval of width kT is given by

$$N_t (E_{Fn}) \, kT = \tau_d \cdot \frac{n}{c} \tag{7}$$

The stationary values of electron density plotted in Figure 19 are those from which the decays were measured. The decay times are given in Figure 16. The values beside the measured points

in Figure 19 indicate the positions of the Fermi level. In
Figure 20 the trap distribution as calculated from Eq. (7) is
given in curve (1).

This curve is not in agreement with the trap distribution
as obtained from TSC curves. A reason for that can be the fact
that the lifetime for electrons in the conduction band increases
with proceeding decay of the photocurrent when measured in or
below the superlinear range. Thus curve (1) in Figure 20 is also
an upper limit for the trap distribution. Since the production
of holes near the valence band is stopped with the termination
of optical excitation, and recombination, which under illumination
could go over fast recombination centers, now must proceed to
a larger extent over slow centers (2.05 eV centers), where most
of the holes are trapped, an increase of electron lifetime must
be expected.[*] It is difficult to obtain the actual lifetime of
conduction electrons for the decaying photocurrent; however one
easily can give an upper limit of this lifetime, using the ratio
of the stationary electron densities as actual observed n_{obs}
and as obtained by extrapolation of the linear range at high
excitation, n_{lin}:

$$\tau_{cmax} = \frac{n_{lin}}{n_{obs}} \tau_c \tag{7a}$$

Using τ_{cmax} instead of τ_c in Eq. 7 one obtains a lower limit for

----

[*]There is no thermal equilibrium between trapped holes and
valence band during decay since $E_{F_p} - E_V > E_c - E_{F_n}$ (n-type
photoconductivity) and thermal equilibrium between trapped
electrons and conduction band is only barely fulfilled.

the trap distribution as given in Figure 20, curve (2).[*]   This
curve shows a trap maximum at 0.23 eV in agreement with the TSC
curve analysis and another lower maximum at 0.48 eV which cannot
be separated with TSC. The trap density between 0.2 and 0.3 eV
as obtained from curve (2) is $3 \times 10^{15} cm^{-3}$. This is by a factor
of three lower than the value obtained from TSC curves, using a
gain factor as obtained from the stationary photoconductivity.
However, for the same reason, τ_c for TSC curves is larger than
for stationary photoconductivity, and, using a similar estimation
as for decay curves one obtains $G(-135^{o}C) \simeq 100$ and herewith
$N_t(0.23) \simeq 5 \times 10^{15} cm^{-3}$ from TSC curve (1) in Figure 17. This
is in good agreement with the decay curve analysis.

The unusual behavior of the TSC curves, namely that the
current changes by up to four orders of magnitude due to different
pre-irradiations may also be explained by assuming a change in
τ_c and thereby in the gain factor, down to a lowest value of
$G(-135^{o}C) = 10^{-2}$ after intensive irradiation at $25^{o}C$. These
changes in the gain factor might be attributed to photochemical
reactions[13] or photo induced absorption of oxygen[29], or to the
fact that at elevated temperatures another group of deep traps
(repulsive centers) can be filled, which lie close to 0.65 eV,
and therefore does not show up in TSC curves. Such trapping forces
the hole density in the 2.05 eV hole trap to increase because of
quasi-neutrality and therefore enhances the recombination. This

---

[*]Since at higher temperatures the intensity could not be in-
creased into the linear range, the photoconductivity there is
estimated for all temperatures to approach the linear range of
the $-180^{o}C$ curve.

results also in an overshoot of rise curves at elevated temperatures, which is observed (Figure 14, Curve 5). Assuming the latter explanation, the density of repulsive deep traps N_{td} can be estimated from

$$N_{td} \simeq \frac{\delta a_o \tau_2}{h} \tag{8}$$

where τ_2 is the time of the inflection point after the maximum in an overshoot rise curve (curve 5) for $\delta = 0.2$, and $a_o = 10^{14}$ photons/cm^{2}s one obtains $N_{td} \simeq 2 \times 10^{18}$cm^{-3}, which is about three orders of magnitude larger than the trap density fillable at lower temperatures, and, according to Eq. 3 causes the density of conduction electrons to decrease by a similar amount in agreement with the experimental behavior given in Figure 17, curve (6).

However from the experimental results photochemical reactions cannot completely be excluded as possible explanation since they would lead to a similar behavior.

Photoinduced absorption of oxygen is the least probable explanation of the entire reduction of the gain factor, since measurements were taken at 10^{-3} torr and changes of the conductivity over several orders of magnitude are observed at high oxygen pressures only.[28]

At low excitation densities the rise curves show a plateau from which the trapping cross section for electrons S_n, can be obtained.[12]

$$S_n = \frac{1}{n_1 \tau_1 v_{th}}$$

with n_1^- = electron density at the plateau, τ_1 = time duration

of the plateau and v_{th} = thermal velocity of the electrons.

From Figure 14 one obtains for the trapping cross sections the

values given in Table 3.

T($^\circ$C)	n_1(cm^{-3})	τ_1(s)	v_{th}(cm/s)	S_n(cm^2)	For traps between (eV)
25°	4 x 10^9	7	2.6 x 10^7	1.4 x 10^{-18}	0.67 and 0.52
-180°	≤5 x 10^7	80	1.5 x 10^7	>2 x 10^{-17}	0.6[*] and 0.2

Table 3

Thermal quenching,[**] partial filling of deep traps and of

traps slightly above the quasi-Fermi level at the plateau

prevents a reliable evaluation of the trap density from rise

curves using a formula similar to Eq. 8 (it leads to values of

N_t between 5 x 10^{15} and 3 x 10^{16}cm^{-3}, which are slightly too

high for shallow traps and too low for deep traps).

Summarizing the results for the electron trap distribution,

at least two distinct levels, one very close to the Fermi level

at about 0.66 eV and with a high density of at least 10^{18}cm^{-3},

and one at 0.23 eV with a density of about 5 x 10^{15}cm^{-3} are

observed. There are some indications of a third trap at about

0.43 eV with a density of about 5 x 10^{13}cm^{-3}. The trap density

between 0.45 and 0.65 eV is less than 10^{13}cm^{-3}. The trap distri-

bution between conduction band and 0.1 eV was not investigated.

----

[*]Before running curve (1) in Figure 12 deep traps were filled
by preceeding irradiation of room temperature.

[**]G.A. Dussel drew my attention to the fact that plateau curves
may be markedly influenced by quenching and a simple evaluation
as proposed in Ref. 12 cannot be conducted in or above the
superlinear range.

The deep trap at 0.66 eV is a repulsive center with a capture cross section of about $10^{-18} cm^2$ and can be filled only at temperatures above room temperatures. The 0.23 eV trap has a normal capture cross section of $>2 \times 10^{-17} cm^2$.

The low trap density between 0.3 and 0.65 eV is commensurate with the unusually fast response time observed in these layers.

6.4 RECOMBINATION CENTERS

The cross section for recombination of electrons with holes, S_{np}, can be obtained from

$$\frac{dn}{dt} = a - \gamma\, np \simeq a - \gamma n N_t^* \qquad (10)$$

where $\gamma = S_{np} v_{th}$ is the coefficient for recombination, and N_t^* is the density of all levels between the Fermi level and the quasi-Fermi level for electrons and $a = \delta a_o / h$, the number of optically excited electrons/cm^3s, assuming quantum efficiency one. For stationarity it holds

$$S_{np} = \frac{a}{v_{th} n N_t^*} = \frac{1}{\tau_c N_t^* v_{th}} \qquad (10a)$$

Values for the recombination cross section can easily be obtained using the information given in Figures 10 and 19, and are presented in Table 4.

$T(^\circ C)$	$\lambda(m\mu)$ $a(photons/cm^3 s)$	$n(cm^{-3})$ $E_{Fn}(eV)$	$N_t^*(cm^{-3})$ $\tau_c(s)$	$S_{np}(cm^2)$
25°	515 1.8×10^{17}	1.3×10^{12} 0.37	$\lesssim 2 \times 10^{18}$ 7×10^{-6}	2×10^{-20}
-180°	495 4×10^{16}	2×10^{13} 0.1	$\lesssim 2 \times 10^{18}$ 1.5×10^{-4}	2×10^{-22}

Table 4

These capture cross sections are effective parameters
for the recombination processes and indicate photoelectric acti-
vation. However, since at ~180°C the majority of holes are
captured at the 2.05 eV level, it can be assumed that the tabu-
lated value is the cross section for electron recombination at
these levels, $S_{np}(2.05) = S_n(2.05) \lesssim 2 \times 10^{-22} cm^2$.

6.5 OPTICAL ABSORPTION IN THE EXTRINSIC RANGE

The optical absorption at wavelengths above 530 mμ is too
small to be measured directly. However, some information about
the photoelectric active absorption K_{pel} can be obtained from
the long-time rise curves (plateau curves). Assuming that the
quantum efficiency is independent of the wave length, and the
trapping probability is much higher than the recombination prob-
ability, the time necessary to fill the traps after start of
optical excitation is a measure of the absorption. From the
rise curve at known absorption (495 mμ) in Figure 14 one obtains
the density of traps. The absorption at longer wavelengths is
then given by

$$K_{pel}(\lambda) = K_{pel}(495)\frac{\mathcal{T}_1(495)a_0(495)}{\mathcal{T}_1(\lambda)a_0(\lambda)} \qquad (11)$$

$K_{pel}(495)$, the absorption constant at 495 mμ is equal to $2.2 \times 10^3 cm^{-1}$
from a measured 20% absorption in a layer 10^{-4}cm thick. At a
(495) = 3.1×10^{11} photons /cm^{2}s, the length of the plateau is
$\mathcal{T}_1(495)$ = 80s. From curves (2) and (3) in the same figure, one
obtains $\mathcal{T}_1(750)$ and $\mathcal{T}_1(800)$; and with corresponding values of
a_0 given in the captions, one calculates from Eq. (11) $K_{pel}(750) =$
2 cm^{-1}, K_{pel} (800) = 1 cm^{-1}. Similarly $K_{pel}(1.3\mu) = 0.25$ cm^{-1}

was calculated.

The total absorption is higher than these values by an unknown fraction because of photoelectric inactive absorption processes in the infrared. However, up to possibly 800 mμ, K_{pel} gives at least the order of magnitude of total absorption.

6.6 SURFACE PROPERTIES

From the steep decrease of the photocurrent at the band edge one may conclude to an enhanced recombination near the surface either because of an increased density of recombination centers, or because of centers with higher recombination cross section. The slow-rise curve at 350 mμ excitation with 1.5×10^{13} photons/cm^{2}s shows a plateau with $I = 3.5 \times 10^{-8}$a, $n_1 = 1.4 \times 10^{11}$cm^{-3} and $\tau_1 = 0.3$ s, indicating 5×10^{12} traps/cm^2 at the surface. These traps have a capture cross section of about 2.5×10^{18}cm^2. This favors the first explanation.

The lifetime of electrons in the surface-near region is decreased by about two orders of magnitude as compared to the lifetime of electrons in the bulk: at wavelengths below 490mμ (for 25°C) and 470 mμ (for -180°C) these lifetimes are $\tau(25^{\circ}C) = 2 \times 10^{-8}$s, and $\tau(-180^{\circ}C) = 2 \times 10^{-6}$s. The steeper decrease of photoconductivity at the band edge at 25°C as compared to -180°C may be understood by phonon assisted recombination in the surface-near region.

After preparation of the layers there was no attention focused on surface treatment.

7. CONCLUSION

Heat treatment of evaporated CdS layers at 620° to 650°C in an N_2 atmosphere containing HCl, copper, cadmium, sulfur, and traces of oxygen result in a significant improvement of photoelectric properties. This is attributed to recrystallization under conditions which allow a supply of intrinsic material and favorable doping at temperatures low relative to the growth temperature of single crystals. Chlorine and copper are used for doping the layer, cadmium and sulfur to prevent evaporation and to supply material for annealing of defects.

HCl is probably also used for material transport over the gas phase. This procedure is known and is used at slightly higher temperatures for single crystal growth.[14] The temperature is kept low enough that substantial growth or evaporation of the layers does not yet occur. However, these conditions seem sufficient to allow growth at surface defects, such as grain-boundaries, grooves, and edges where crystal growth is enhanced, and which would otherwise usually associate to macroscopic defects, e.g. pin holes, during recrystallization.

The process of recrystallization is possibly enhanced by copper as observed by Gilles and van Cakenberghe.[6]

The influence of a trace of oxygen during recrystallization is not yet clear. It is known that oxygen incorporated into the lattice in some respects acts similar to copper:[21] it forms a level in the lower part of the band gap and decreases dark- and photoconductivity[22] but increases the L/D ratio, while oxygen

absorbed at the surface may deteriorate the photosensitivity and speed of response (observed for "undoped" crystals[23]). On the other hand, here it may merely be used during the heat treatment to shift the equilibrium in the partly dissociated gas. This, e.g., would reduce the amount of free hydrogen, which is disadvantageous for formation of layers with fast response time, since it produces sulfur vacancies. It also may enhance recrystallization as indicated in [26]. The latter explanations are favored.

The level distribution in the band gap as observed in a layer recrystallized by the described method, and with a very short response time at still relatively high photosensitivity, is given in Figure 21. In the investigated range between 0.17 and 2.4 eV five maxima were observed at 0.23, 0.43, 0.67, 1.05, and 2.05 eV. Their density between 0.65 eV and 0.3 eV is less than $10^{13} cm^{-3}$ and is considerably lower than that known for other evaporated or sintered layers. It is especially interesting that there exists a deep valley in the trap distribution between 0.45 and 0.65 eV with fewer than 10^{12} traps/cm^3 contributing to the short response time of these layers.

The photoconductivity peak at 580 m is generally attributed[16] to a copper center and agrees with our observations. Since this center is observed at higher doping densities only,[17] copper associates may be responsible for the corresponding 2.05 eV hole trap and could be the $(Cu_{Cd}Cu_{Cd})$ "center.* The repulsive

----

*The high dissociation energy of S_2 molecules favors divacancies of Cd which could be occupied by Cu via $(V_{Cd}V_{Cd})$ " + 2 Cu $(Cu_{Cd}Cu_{Cd})$ " which, in turn can easily be ionized. Evidence for the double negative charge is the small capture cross section for electrons and the large cross section for holes.

trap at 0.66 eV may possibly also be attributed to a negatively charged Cu-center, i.e. to Cu_{Cd}'. The 1.05 eV center may then be identified with a copper-donor associate since it does not occur without Cu-doping, and acts as recombination center. Quenching centers[19] always observed in CdS crystals with a quenching energy of 0.9 and 1.3 eV (i.e., about 1.1 and 1.5 eV from the conduction band) are not detectable in these layers. Also the center, usually associated with sulfur vacancies,[17, 19] producing a TSC maximum at about room temperature, is present in a density of less than $10^{12} cm^{-3}$. Since both centers are attributed to intrinsic defects, this indicates that the recrystallization at temperatures below the temperature of the formation of single crystals, and under conditions which supply intrinsic material may cause this low intrinsic defect density. This is turn seems to be responsible for the good photoelectric properties of these layers, which actually surpass those of single crystals.

The chlorine level should lie[20] at about 0.03 eV. The methods used did not allow for its direct observation.

It is remarkable that in many respects these layers resemble closely CdSe which also shows similarly fast response time, a pronounced superlinearity of the photoconductivity vs. light intensity, and no quenching at room temperature.[15]

ACKNOWLEDGEMENTS

REFERENCES

1. H. Berger, Phys. Stat. Sol. $\underline{1}$, 739 (1961).

2. H. Berger, E. Gutsche and W. Kahle, Phys. Stat. Sol. $\underline{7}$, 679 (1964).

3. C. A. Escoffery, J. Appl. Phys. $\underline{35}$, 2272 (1964).

4. M. G. Miksic, E. S. Schlig and R. R. Haering, Sol. St. Elec. $\underline{7}$, 39 (1964).

5. Y. Sakai and H. Okimura, Japan J. Appl. Phys. $\underline{3}$, 144 (1964).

6. J. M. Gilles and J. Van Cakenberghe, Nature $\underline{182}$, 862 (1958)

7. T. K. Lakshamanan and J. M. Mitchell, Trans, Amer. Vac. Soc. Symp., 335 (1963).

8. J. Dressner and F. V. Shallcross, J. Appl. Phys. $\underline{34}$, 2390 (1963).

9. A. Vecht and A. Apling, Phys. Stat. Sol. $\underline{3}$, 1238 (1963).

10. H. Berger, Phys. Stat. Sol. $\underline{1}$, 739 (1961).

11. E. Spenke, <u>Electronic Semiconductors</u>, (McGraw-Hill Co., New York, 1958).

12. K. W. Böer, H. Vogel, Ann. Phys. $\underline{17}$, 10 (1955).
    K. W. Böer, H. Wantosch, Ann. Phys. $\underline{7}$, 406 (1959).

13. K. W. Böer, W. Borchardt, E. Borchardt, Z. Phys. Chem. $\underline{203}$, 145 (1954).
    W. Borchardt, Phys. Stat. Sol. $\underline{2}$, 1575 (1962).

14. R. H. Bube, E. L. Lind and A. B. Dreeben, Phys. Rev. $\underline{128}$, 532 (1962).

15. R. H. Bube, Phys. Rev. $\underline{99}$, 1105 (1955)

16. W. Keith, Z. Angew. Phys. $\underline{7}$, 1 (1955).

17. R. H. Bube, and L. A. Barton, RCA Review, 564 (1959).

18. R. G. Bube, J. Appl. Phys. $\underline{35}$, 586 (1964).

19. J. K. Skarman, Sol. St. Electr. $\underline{8}$, 17 (1965).

20. R. H. Bube, J. Chem. Phys. $\underline{23}$, 18 (1955).

21. G. Kuvabara, J. Phys. Soc. Japan $\underline{9}$, 97 (1954).

22. W. Muscheid, Ann. Phys. Lpz. $\underline{13}$, 322 (1953).

23. P. Mark, J. Phys. Chem. Sol. $\underline{25}$, 911 (1964).

24. H. Berger, K. W. Böer, and E. H. Weber, Z. Phys. $\underline{158}$, 501 (1960).

25. A. S. Esbitt, Phys. Stat. Sol.

26. H. Berger, E. Gutsche and W. Kahle, Phys. Stat. Sol. $\underline{7}$, 679 (1964).

27. R. H. Bube, Stanf. Univ., Dept. Mat. Sci. Rep. 65-19.

28. P. Mark, J. Phys. Chem. Sol. $\underline{26}$, 959 (1965).

FIGURE CAPTIONS

Figure 1: Schematic of the apparatus for heat treatment of CdS layers; F = calibrated flowmeter, V = valve, D = drying tube.

Figure 2: Photocurrent, dark current, and temperature as a function of the position in the treatment furnace (0 cm indicates the edge of the CdS layer closest to the gas outlet).

Figure 3: Photocurrent and dark current of CdS films treated at 630°C as a function of HCl flow rate.

Figure 4: Photocurrent and dark current of CdS layers treated at 630°C as a function of volume percent oxygen in the nitrogen carrier gas; a) with 7% HCl flow rate and 15 g copper; b) without HCl or copper.

Figure 5: Photocurrent and dark current of CdS layers treated at 630°C as a function of copper spread over the CdS powder in the treatment tube.

Figure 6: Relative optical transmission of CdS layers (normalized to 100% at 540 mμ). (1) untreated layer, evaporated onto 25°C substrate; (2) untreatdd layer evaporated onto 200°C substrate.

Figure 7: Current-voltage characteristic of CdS layer No. 3 with pressed-on indium disk electrodes (white unfiltered light, 250 ft-c).

Figure 8: Photocurrent vs. 1/Temperature (light intensity as parameter). White light with IR cut-off filter (695 mμ cut-off point and 85% transmission in the visible range) and Corning filter Cs 3-74. Applied voltage 1.5 V, electrode distance 2.5 mm.

Figure 9: Photocurrent vs. light intensity (temperature as parameter obtained from curves of Figure 8); (1) and (2) indicate slopes of 1 and 2.

Figure 10: Spectral distribution of the photocurrent at +25°C and at -180°C, applied voltage 12V, electrode distance 2.5 mm. Lower insert: spectral distribution of the photon density at the layer. Upper insert: spectral transparency of the filter Cs 7-57 used at wavelength above 800 mμ; $\circ$ = measured points, $\square$ =corrected values for equal incident photon density.

Figure 11: Decay time of photocurrent as a function of light intensity for white unfiltered light at -180°C and +25°C.

Figure 12: Rise and decay of photocurrent at 25°C and -180°C for 200 ft-c white light with Cs 5-72 and IR cut-off filter.

Figure 13: Decay of photocurrent for differnet layer temperatures and pre-irradiation conditions. (a) all curves are measured at -180°C. If any additional temperature is given, it indicates that immediately before the decay curve was taken, the layer was irradiated with given light at that temperature and cooled under the light down to -180°C.

(1) white unfiltered (400 ft-c, 2600°K), 25°C;
(2) 510 mμ, 9 x 10^{13} photons/cm^{2}s, 25°C;
(3) 510 mμ, 9 x 10^{13} photons/cm^{2}s;
(4) 510 mμ, 9 x 10^{11} photons/cm^{2}s, for one minute after (2);
(5) 500 mμ, 9 x 10^{13} photons/cm^{2}s;
(6) 500 mμ, 8 x 10^{12} photons/cm^{2}s;
(7) 500 mμ, 7 x 10^{11} photons/cm^{2}s;
(8) 775 mμ, 2 x 10^{14} photons/cm^{2}s;
(9) 800 mμ, 2 x 10^{14} photons/cm^{2}s;

(b) decay of photocurrent immediately after irradiation with white light (300 ft-c, 2600°K), filtered with infrared cut-off filter at 25°C and cooling to given temperature.

Figure 14: Rise of photocurrent for different layer temperatures and irradiations:

(1) -180°C, 495 mμ, 3.1 x 10^{11} photons/cm^{2}s;
(2) -180°C, 750 mμ, 2 x 10^{14} photons/cm^{2}s;
(3) -180°C, 800 mμ, 2 x 10^{14} photons/cm^{2}s;
(4) 25°C, 510 mμ, 3.7 x 10^{11} photons/cm^{2}s;
(5) 70°C, 515 mμ, 10^{14} photons/cm^{2}s.

(Note change in scale in curves (4) and (5)).

Figure 15: Decay and rise time of the photocurrent as a function of wavelength (photon density at the layer same as in Figure 10): (a) for -180°C and (b) for +25°C.

Figure 16: Decay time as a function of light intensity for monochromatic irradiation at the band edge (20% absorption point). Family parameter is the temperature.

(1) 25°C, 515 mμ, 6 x 10^{13} photons/cm^{2}s;
(2) -15°C, 510 mμ, 5.8 x 10^{13} photons/cm^{2}s;
(3) -65°C, 505 mμ, 5.6 x 10^{13} photons/cm^{2}s;
(4) -105°C, 500 mμ, 5.3 x 10^{13} photons/cm^{2}s;
(5) -180°C, 495 mμ, 4.9 x 10^{13} photons/cm^{2}s.

The photon densities given above incident to the layer are those for the value 1 in the abscissa.

Figure 17: TSC curves ($1/T > 350 \times 10^{-5}$) and dark current as a function of temperature (stationary values below $1/T = 350 \times 10^{-5}$). Temperature given below indicates the temperature at which after preceeding TSC curve, optical excitation is started and continuously kept on until the next TSC curve;

(1) -180°C, 495 mμ, 10^{12} photons/cm^{2}s;
(2) -180°C, 800 mμ, 2×10^{14} photons/cm^{2}s;
(3) -180°C, 500 mμ, 7×10^{13} photons/cm^{2}s;
(4)   30°C, 515 mμ, 2×10^{12} photons/cm^{2}s;
(5)   30°C, 515 mμ, 2×10^{14} photons/cm^{2}s, excitation for one minute;
(6) repeat of (5) directly following (5) for two minute excitation at 30°C;
(7) 25°C white unfiltered light, (200 ft-c).

Applied voltage 12V, electrode distance 2mm.

Figure 18: TSC curves of Figure 17 redrawn, using Eq. 2a for obtaining the energy scale.

Figure 19: Photocurrent vs. light intensity for monochromatic light at the band edge (20% absorption point) corresponding to the decay measurements given in Figure 16. The values adjacent to the observed current values indicate the position of the Fermi level. (Light intensity as in Figure 16).

Figure 20: Trap distribution as obtained from the analysis of photocurrent decay (Figures 15 and 18). The kT uncertainty is indicated by line segments above the curve.

Figure 21: Level distribution of CdS layer No. 3 measured from photocurrent decay (solid line) and indicated by slow rise curves, spectral distributions of photoconductivity, and thermal quenching (dashed continuation of the curve). The given values of capture cross section are obtained from plateau curves and from the stationary photocurrent with and without thermal quenching.

FIG. 1.

FIG 2.

FIG 3.

PHOTOCURRENT

DARK CURRENT

CURRENT (uA)

LOG % OXYGEN

FIG. 4

PHOTOCURRENT

DARK CURRENT

CURRENT (uA)

10^3
10^2
10^1
10^0
10^{-1}
10^{-2}
10^{-3}
10^{-4}
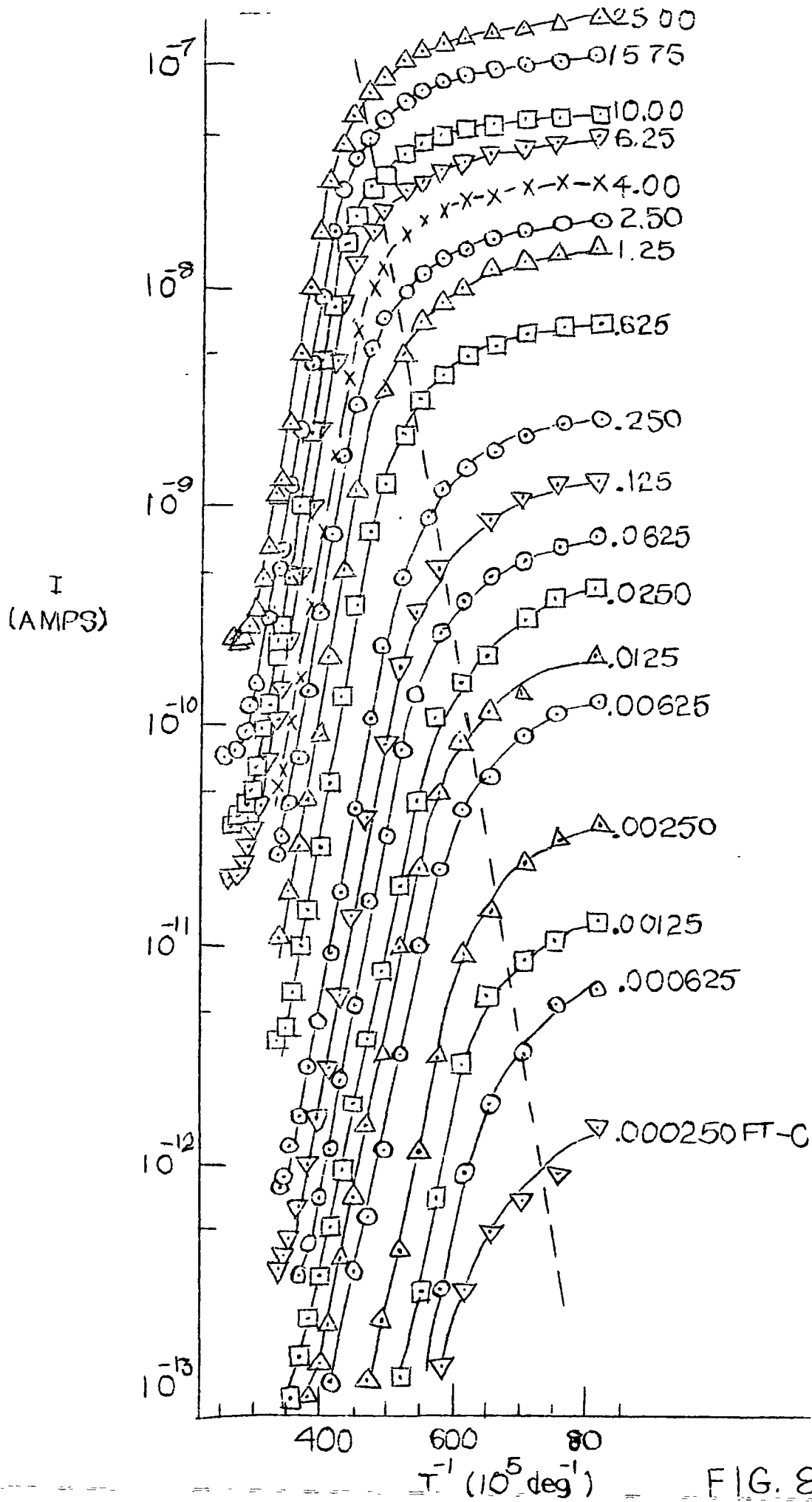10^{-5}
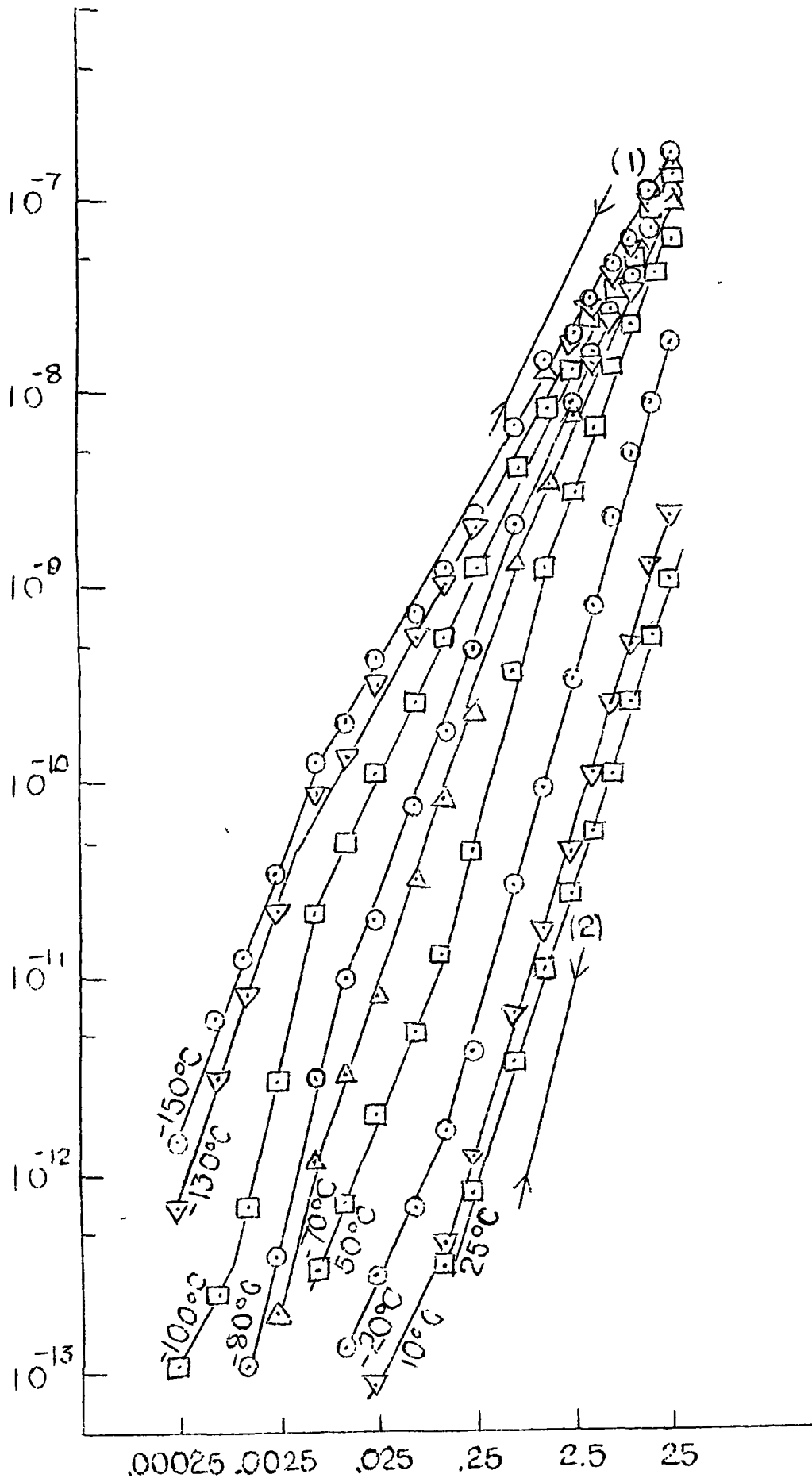10^{-6}

0 15 30 60
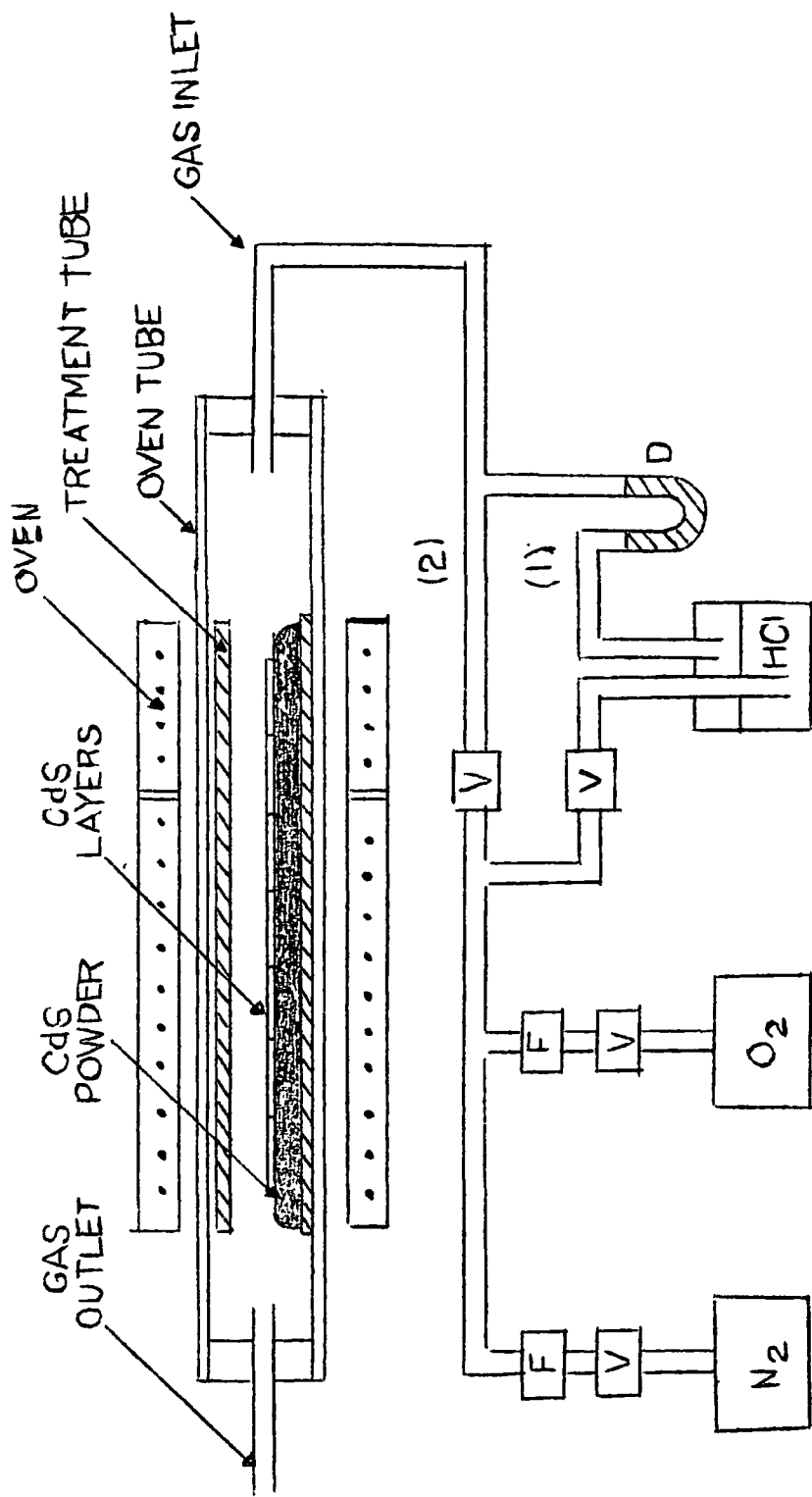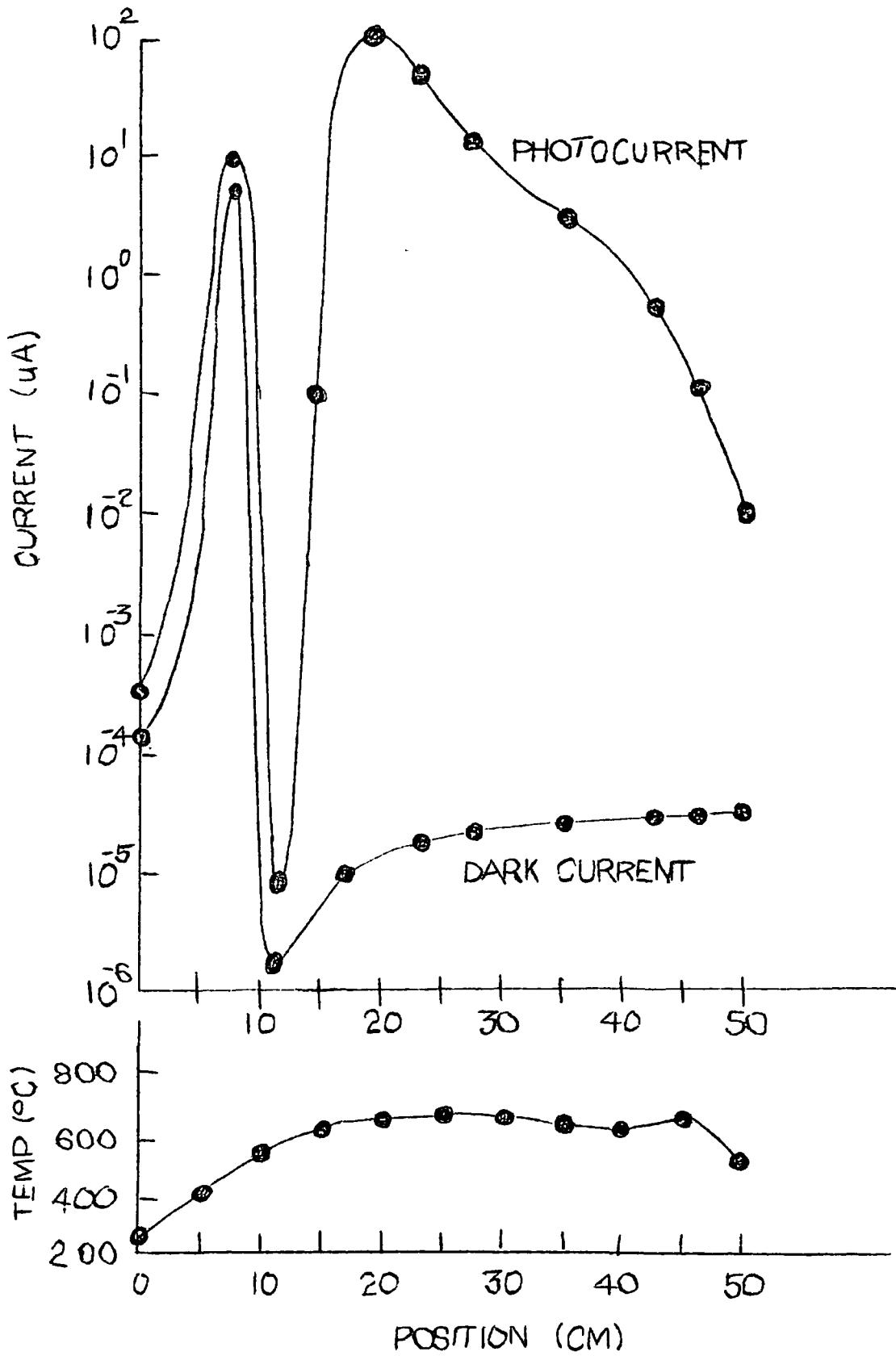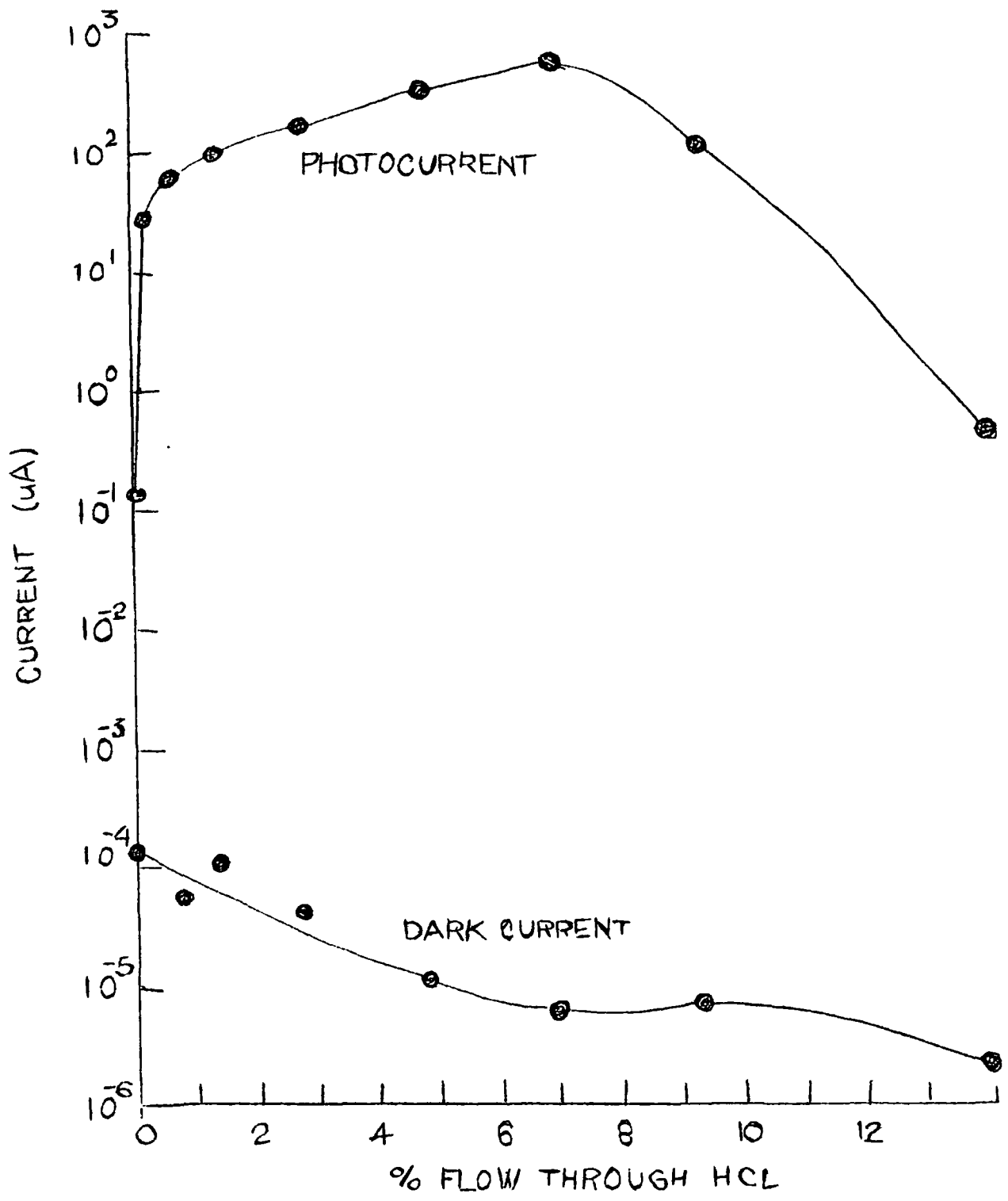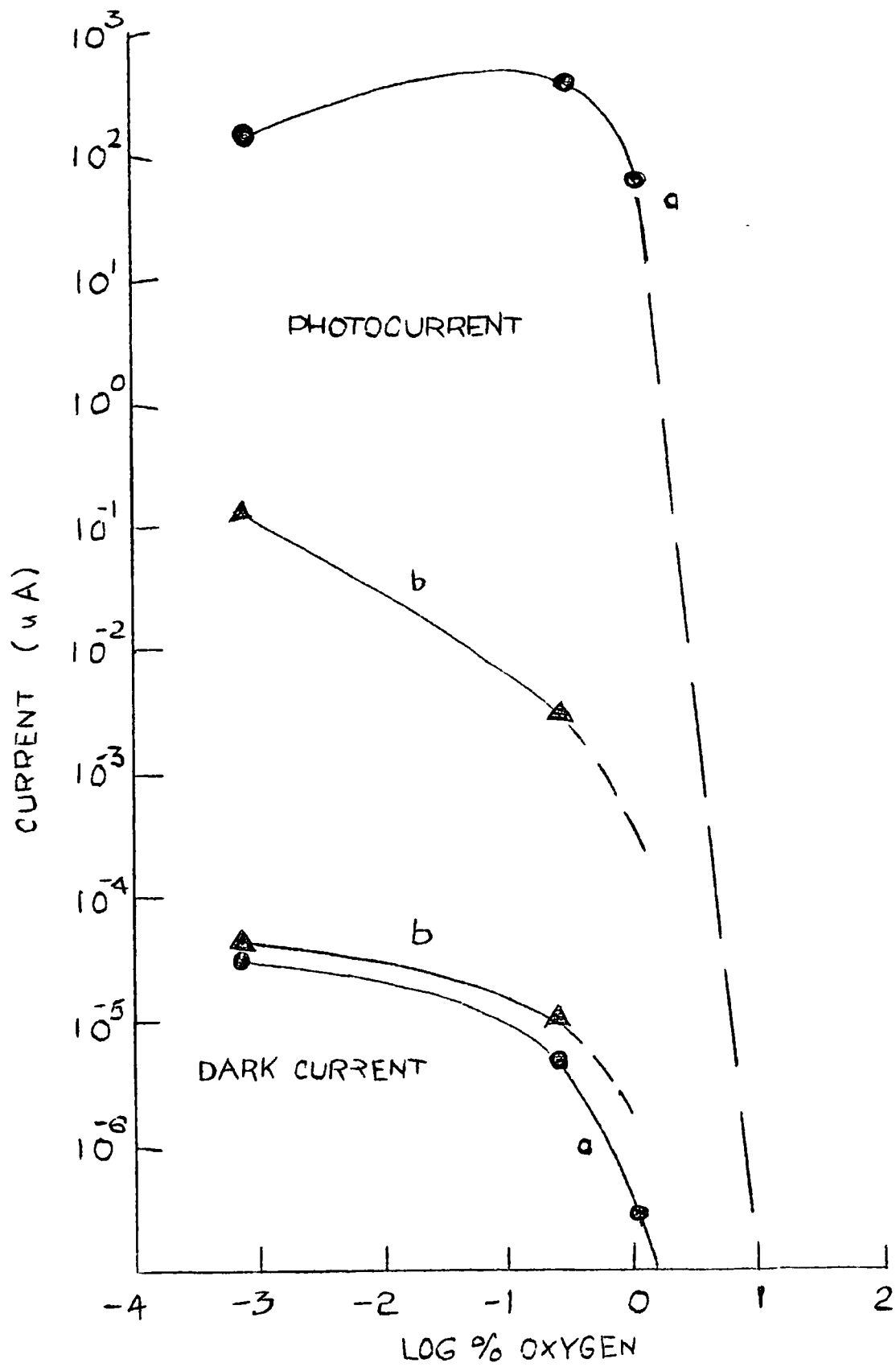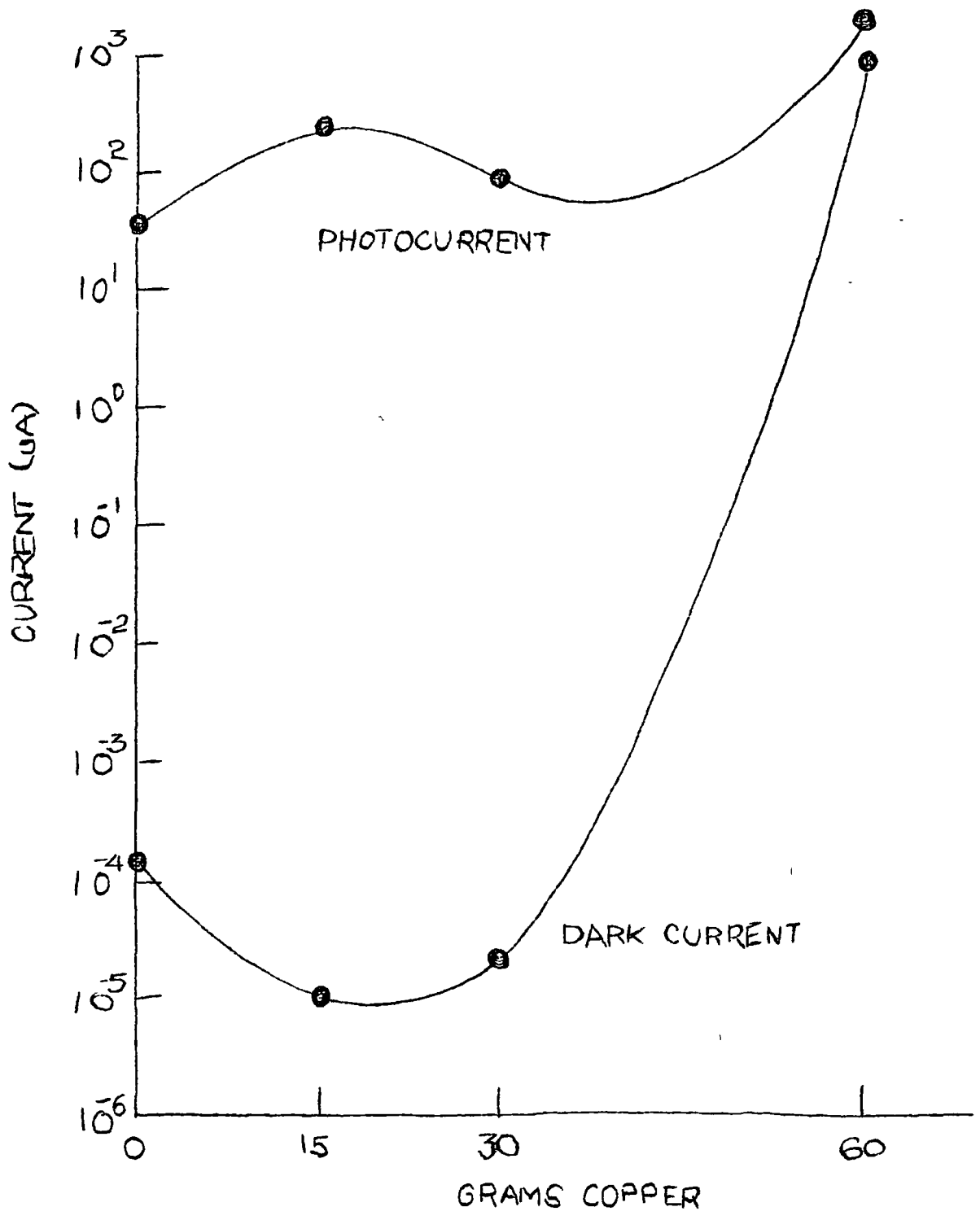
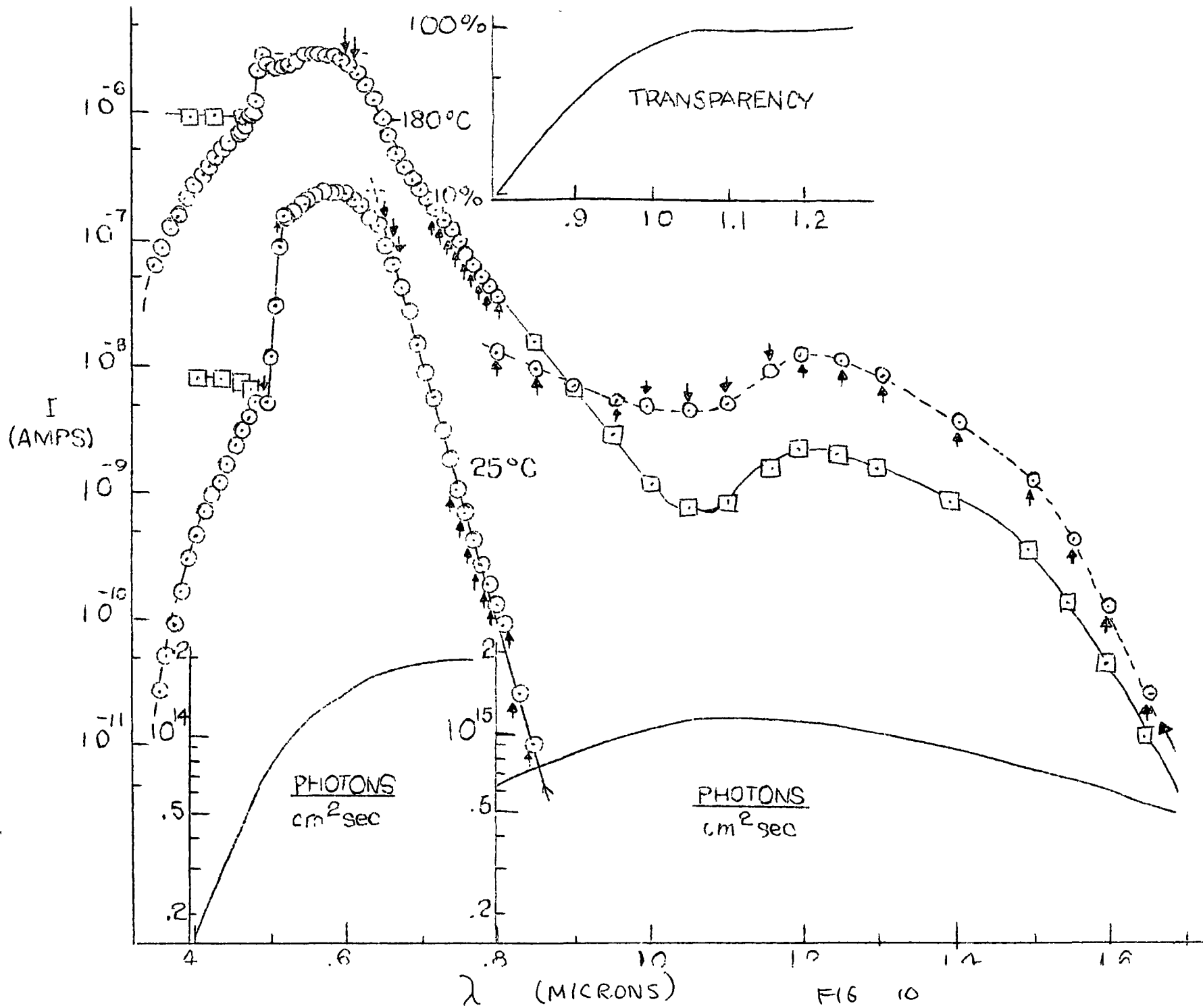GRAMS COPPER

FIG. 5
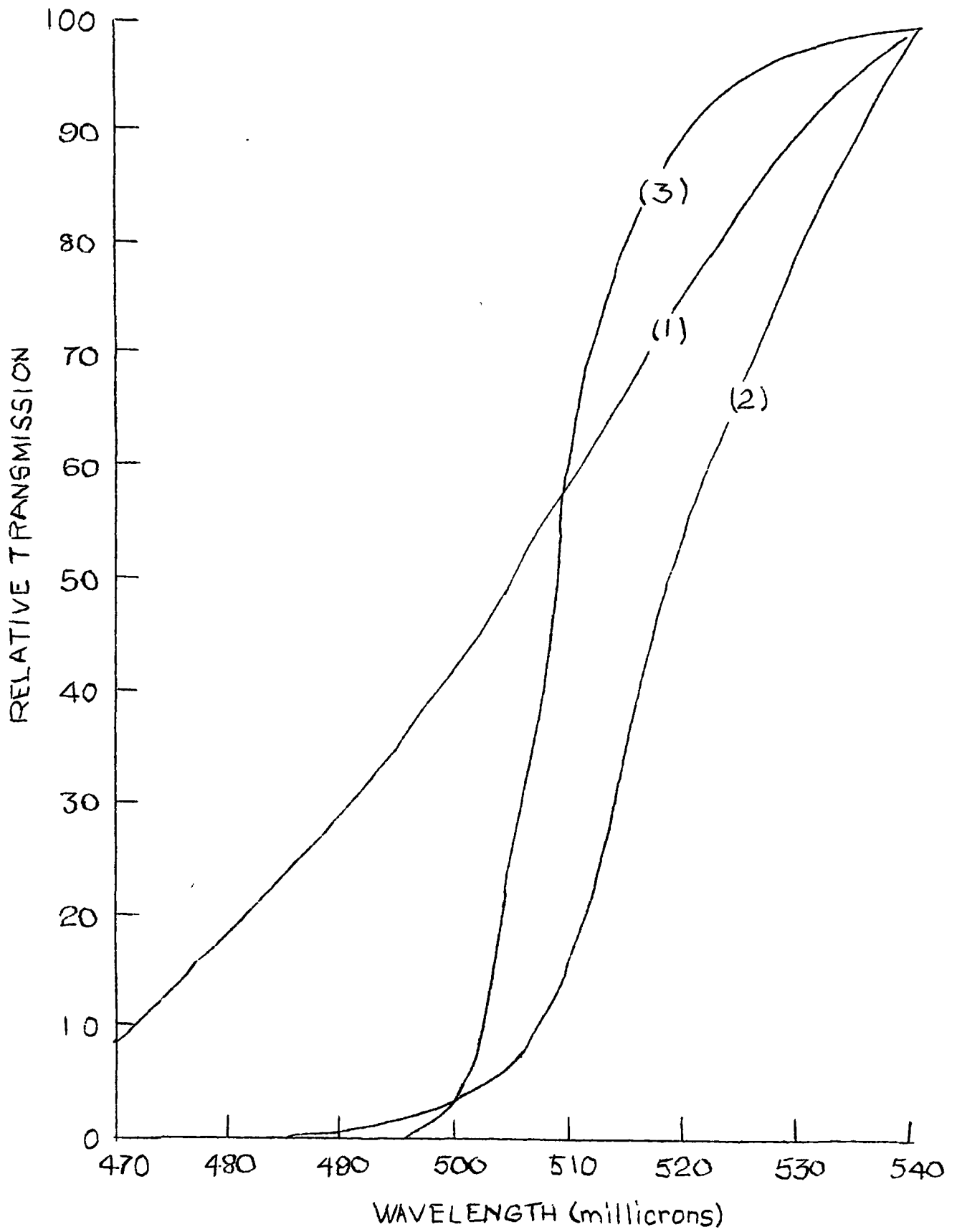
FIG. 6
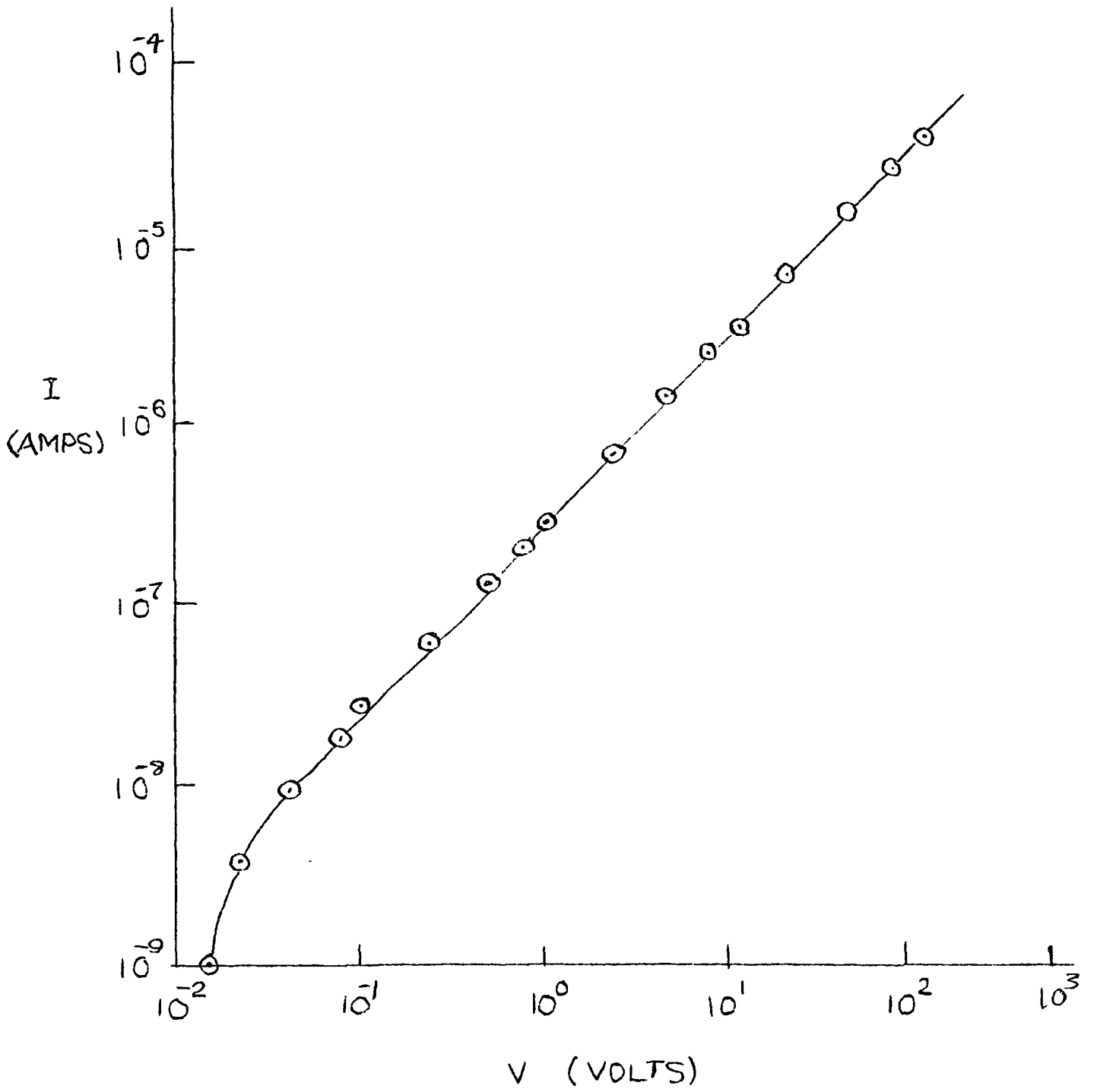
V (VOLTS)

FIG 7

FIG. 8

FIG. 9
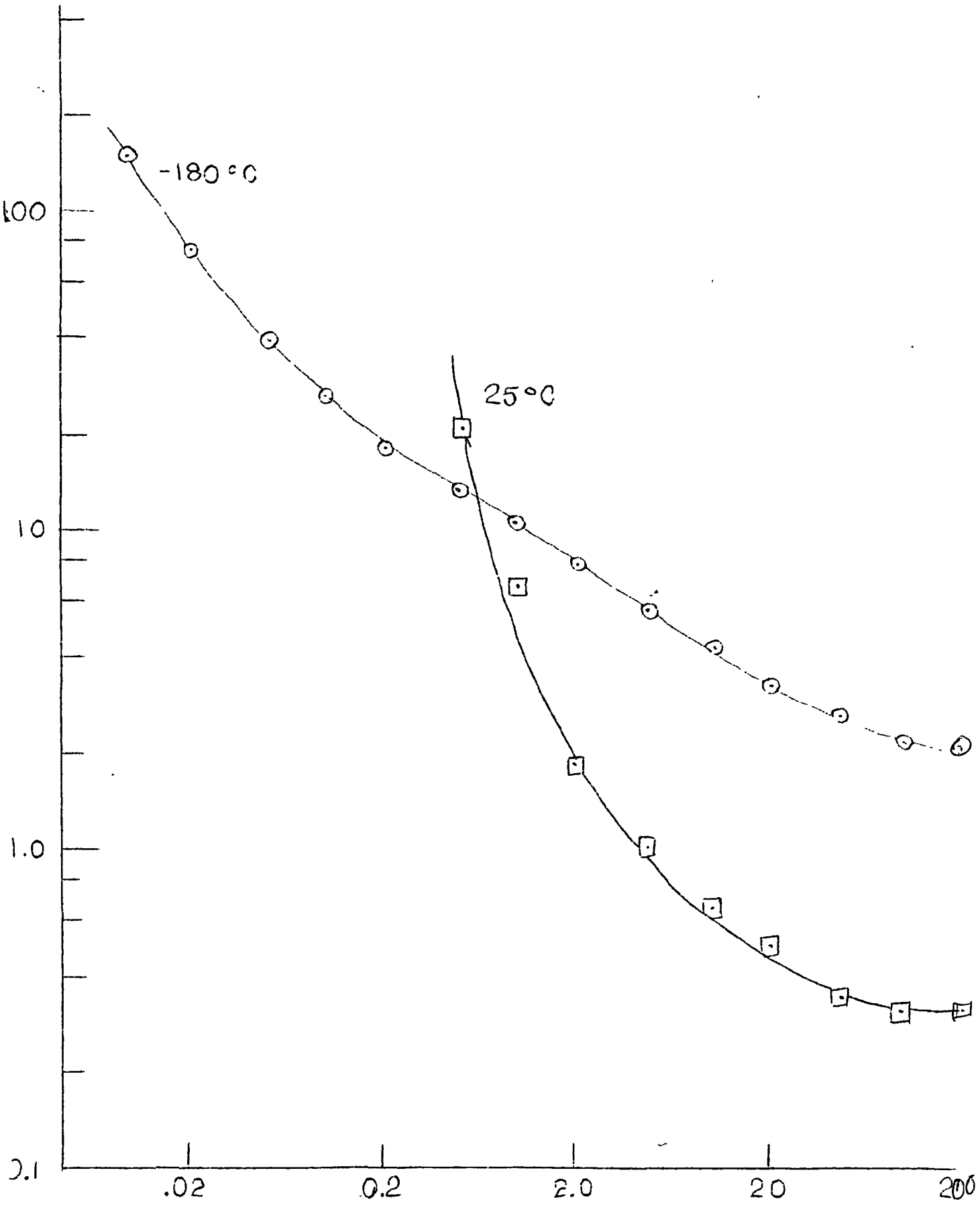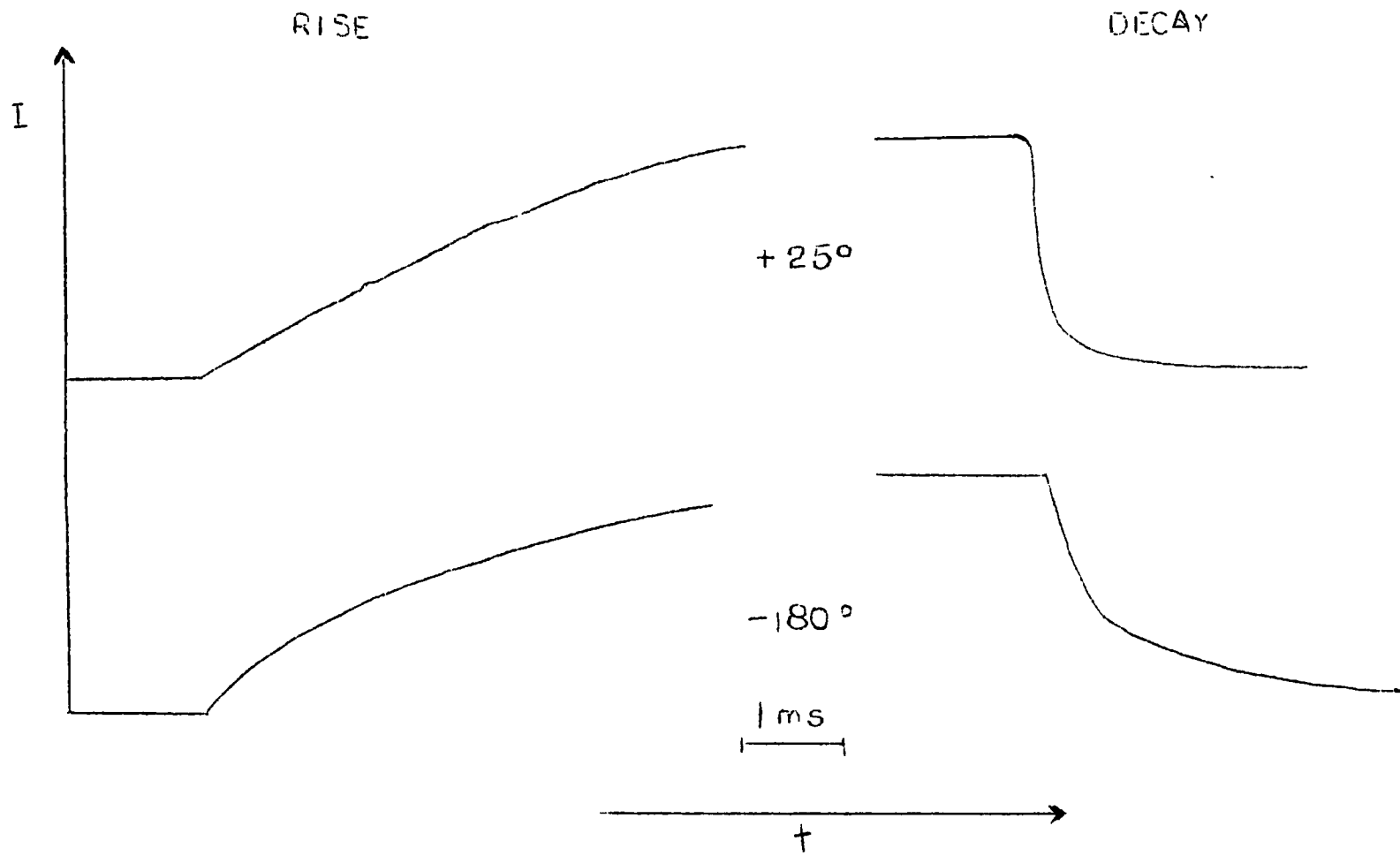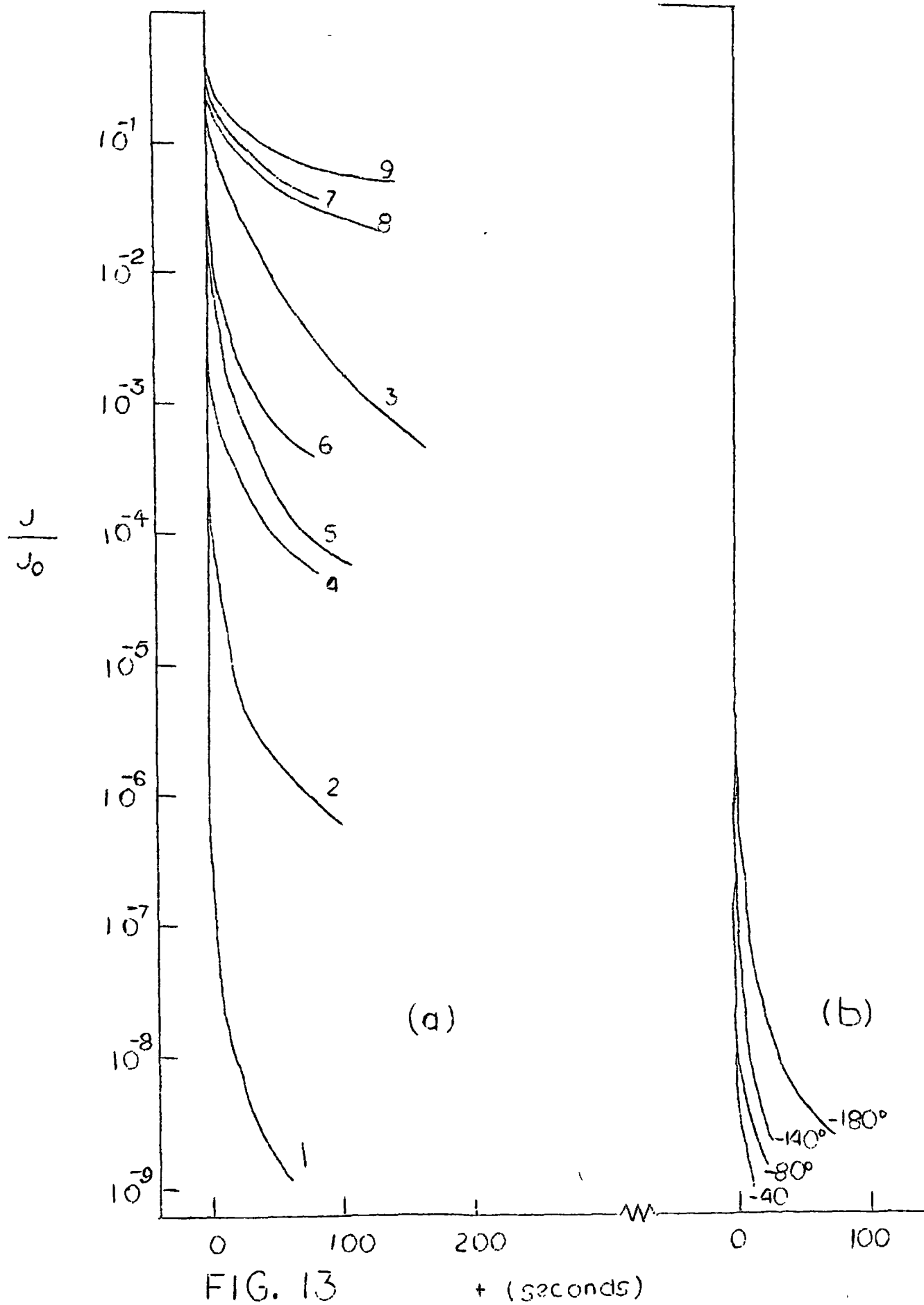
FIG 10

LIGHT INTENSITY (ft.-c.)

FIG. 11

FIG. 12

FIG. 13   + (seconds)
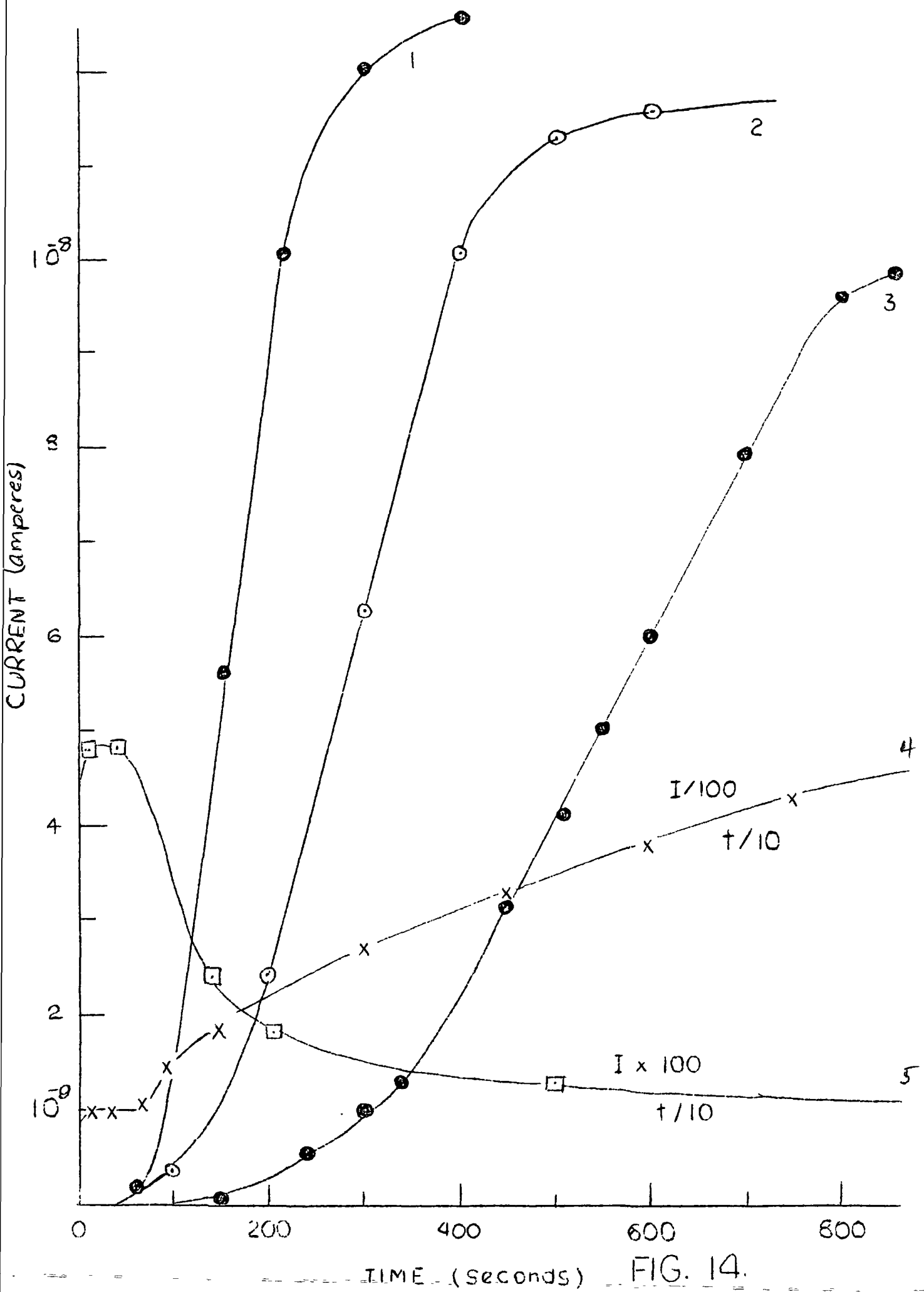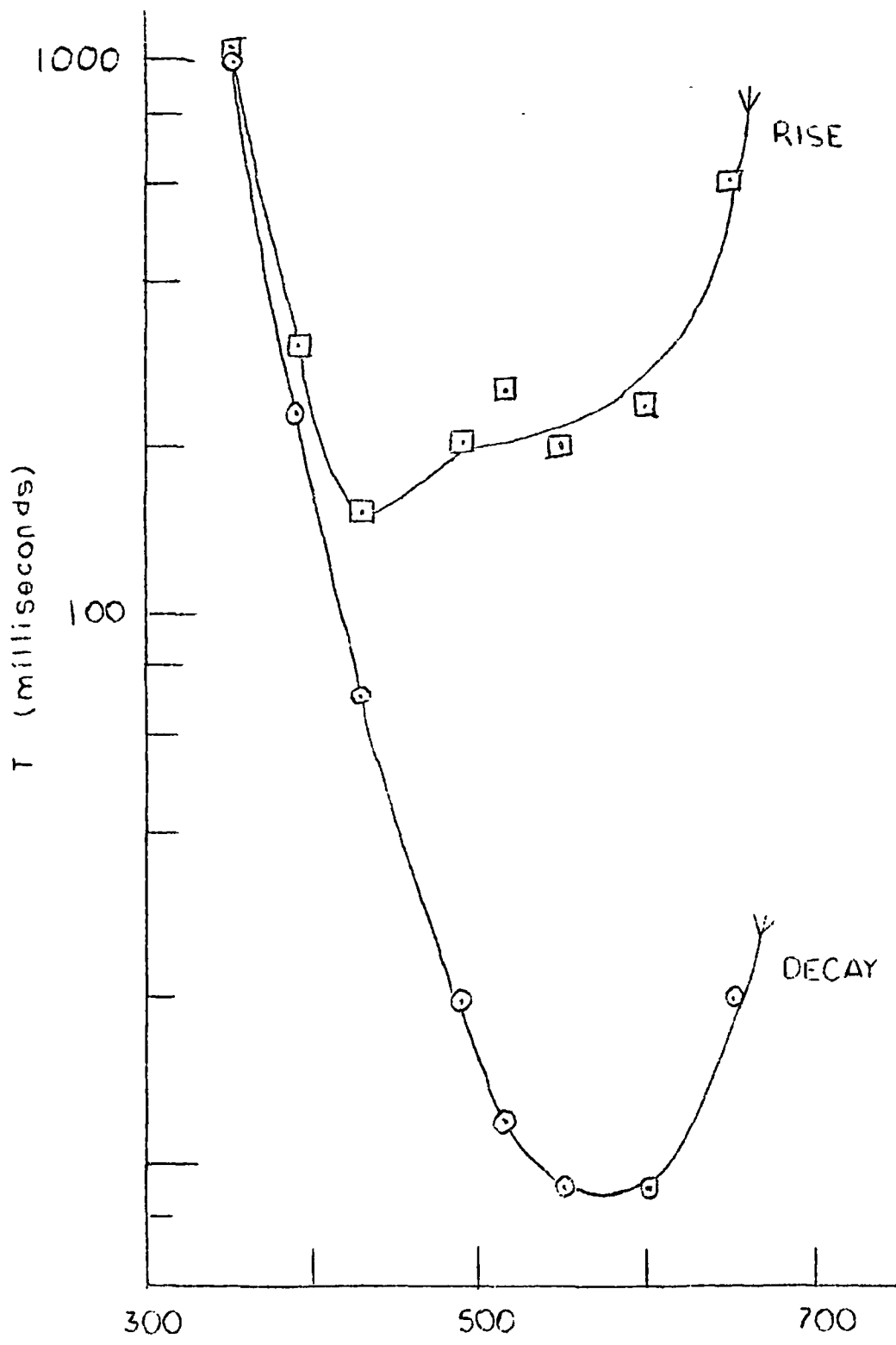
FIG. 14.

FIG. 15a

FIG. 15b

Axis labels: T (milliseconds), WAVELENGTH (millimicrons); curves labeled RISE and DECAY.
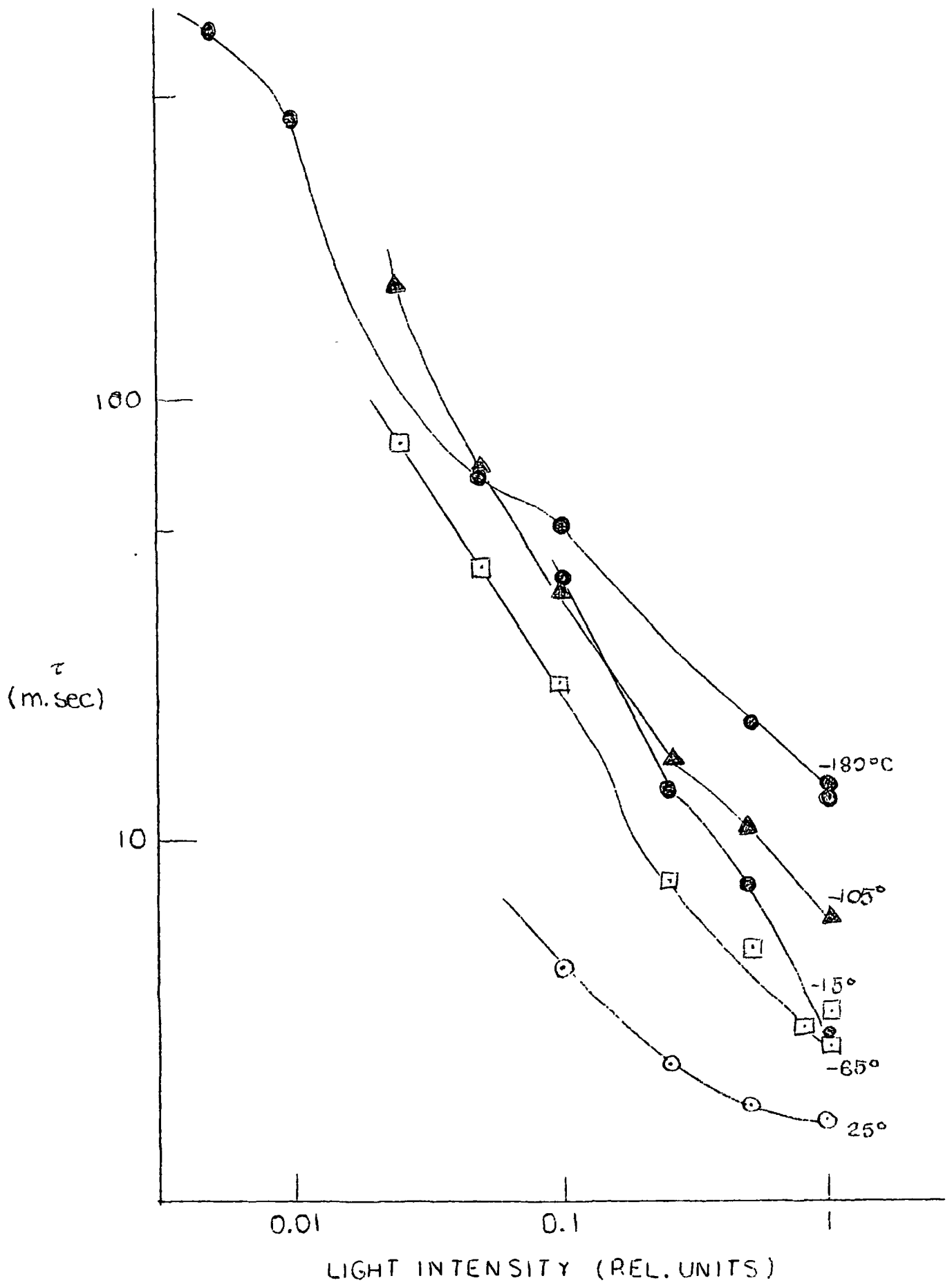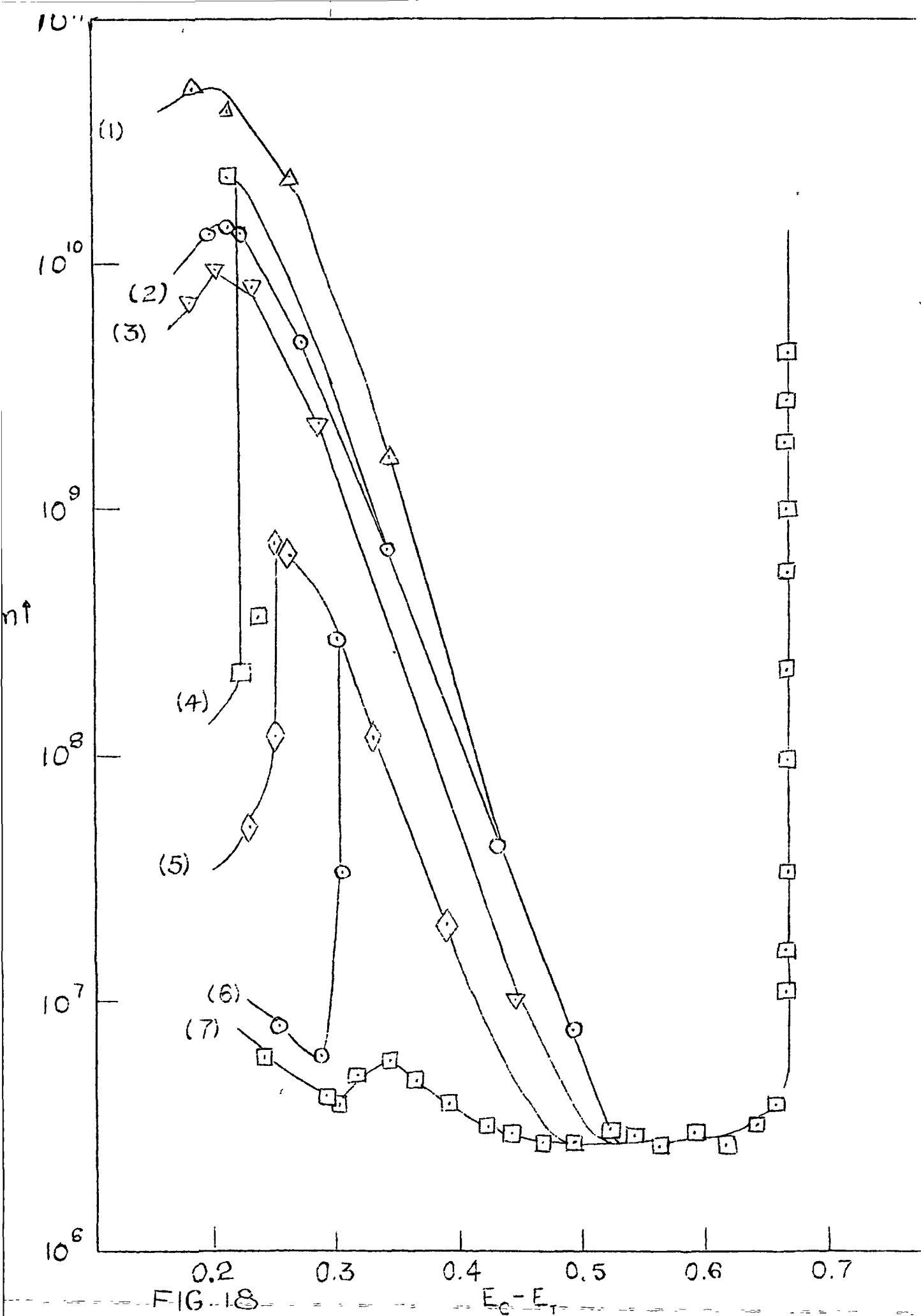
FIG. 16
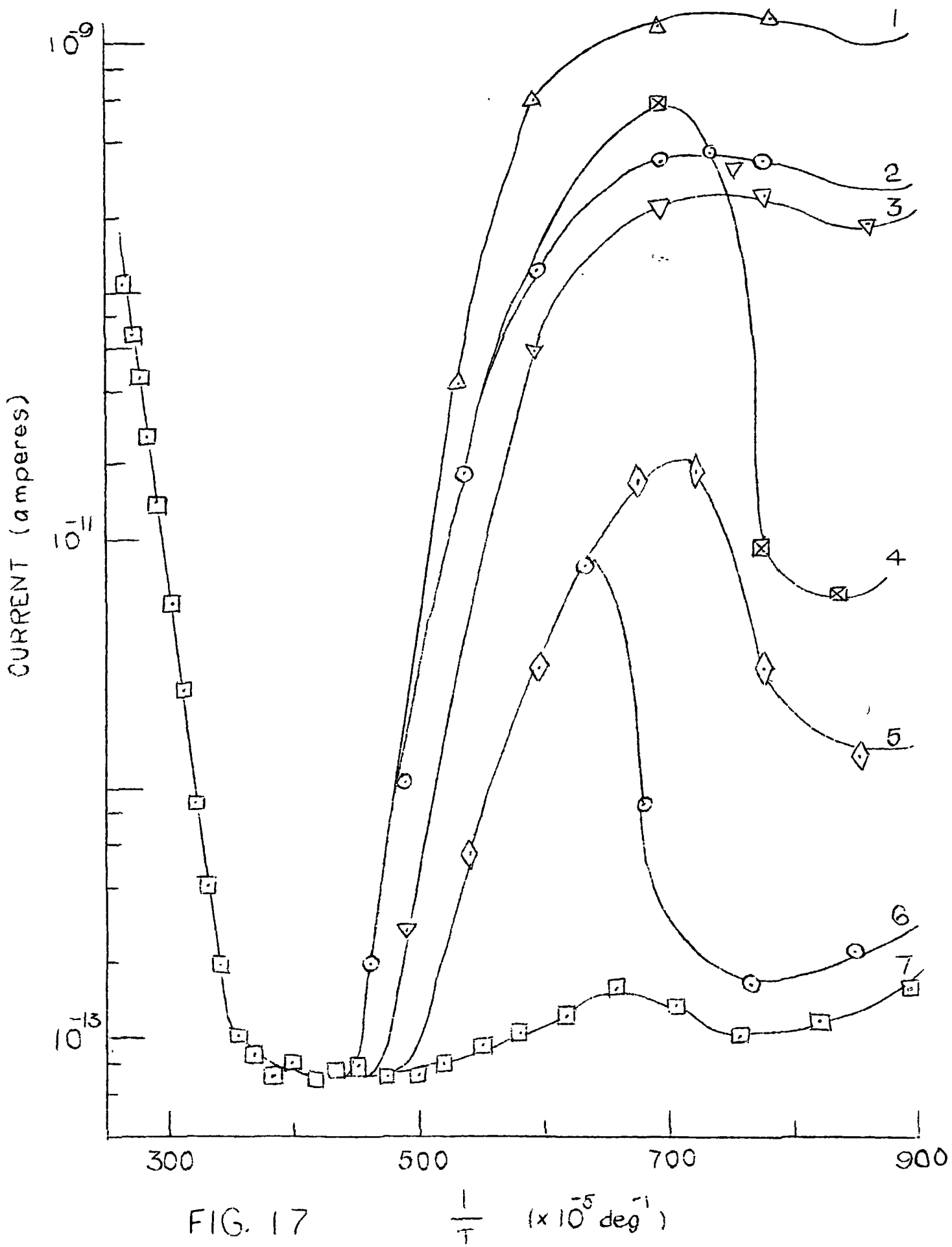
FIG. 17 $\frac{1}{T}$ $(\times 10^{-5} deg^{-1})$

FIG. 18
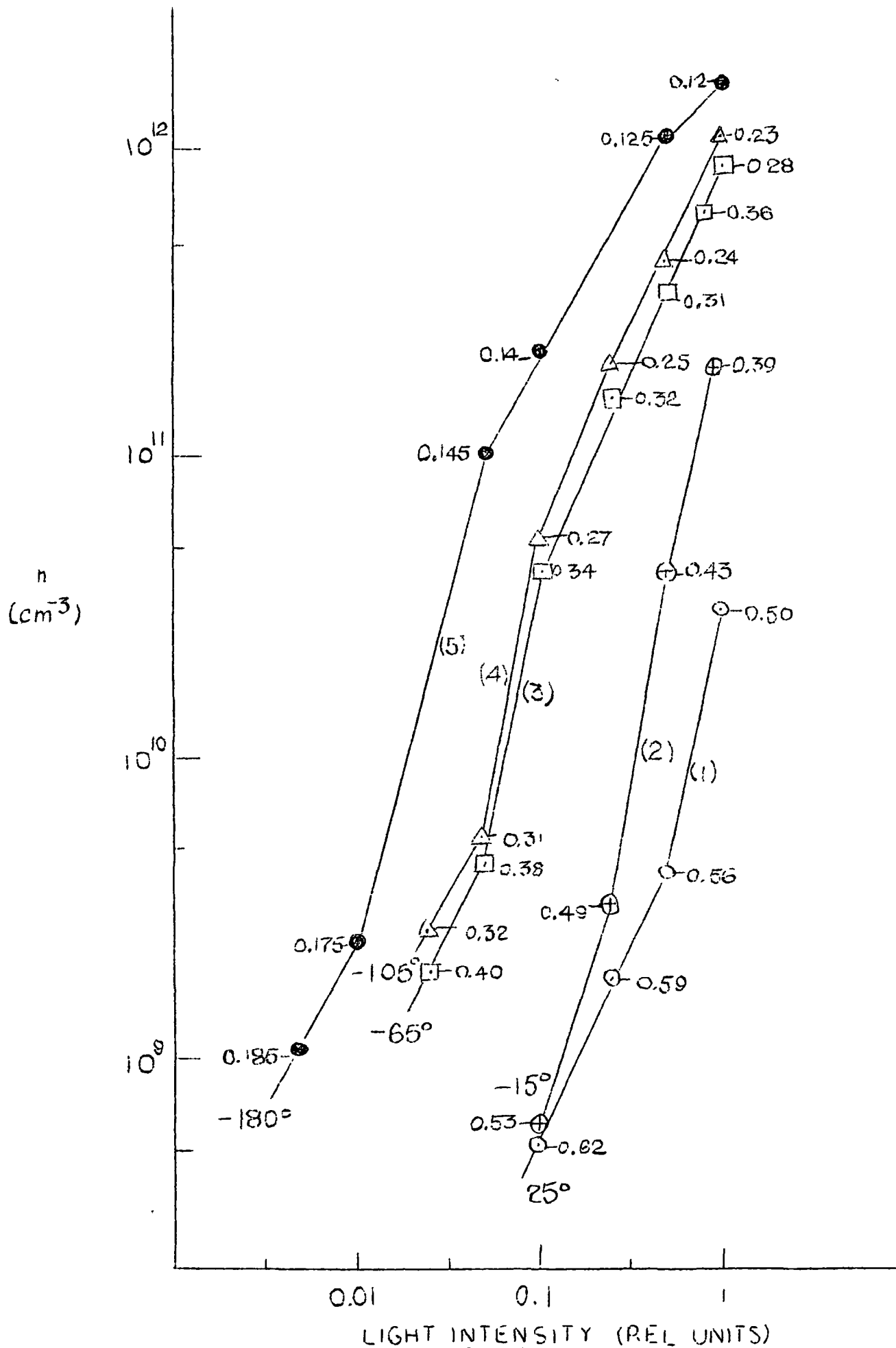
FIG. 19
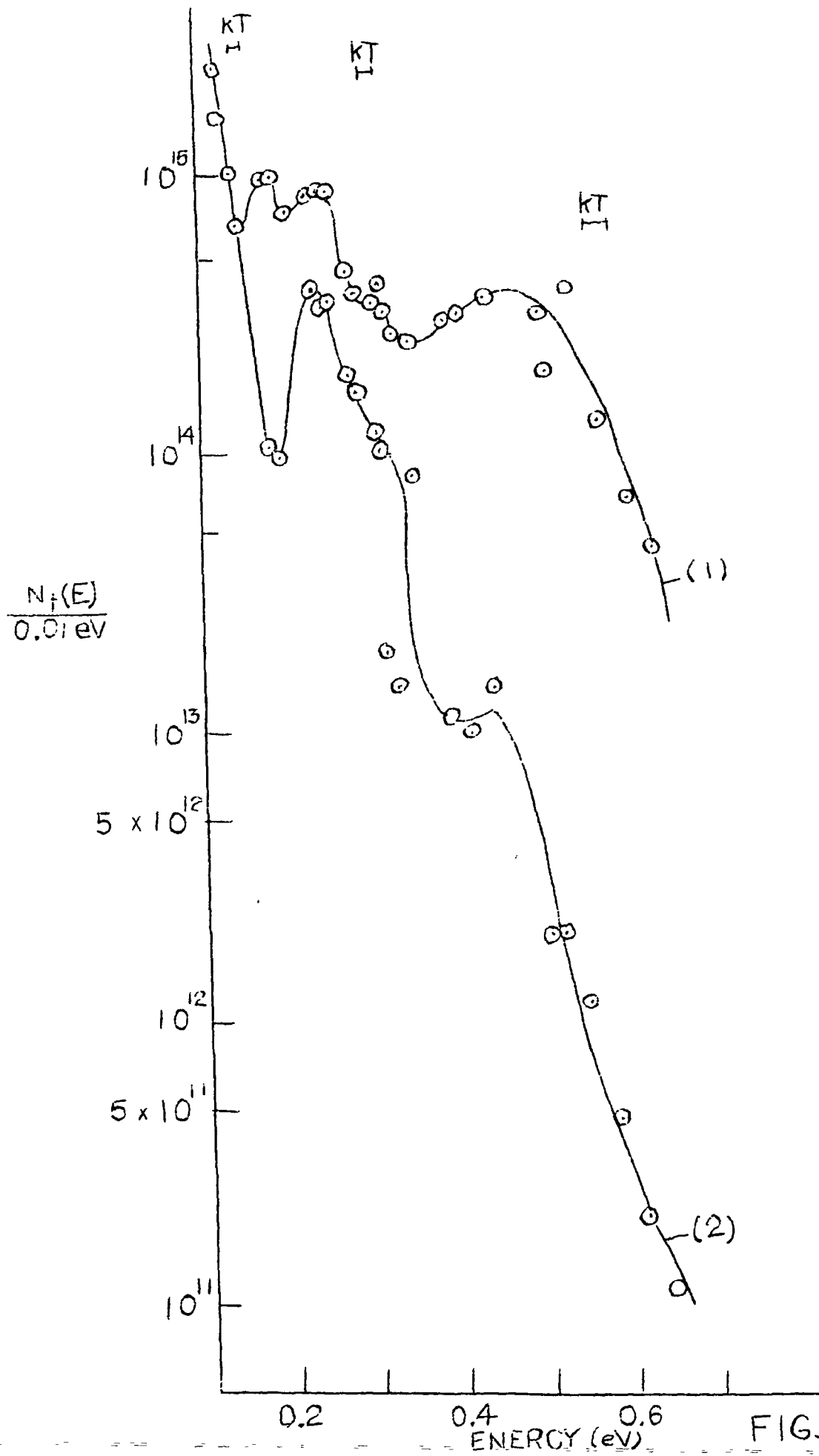
FIG. 20
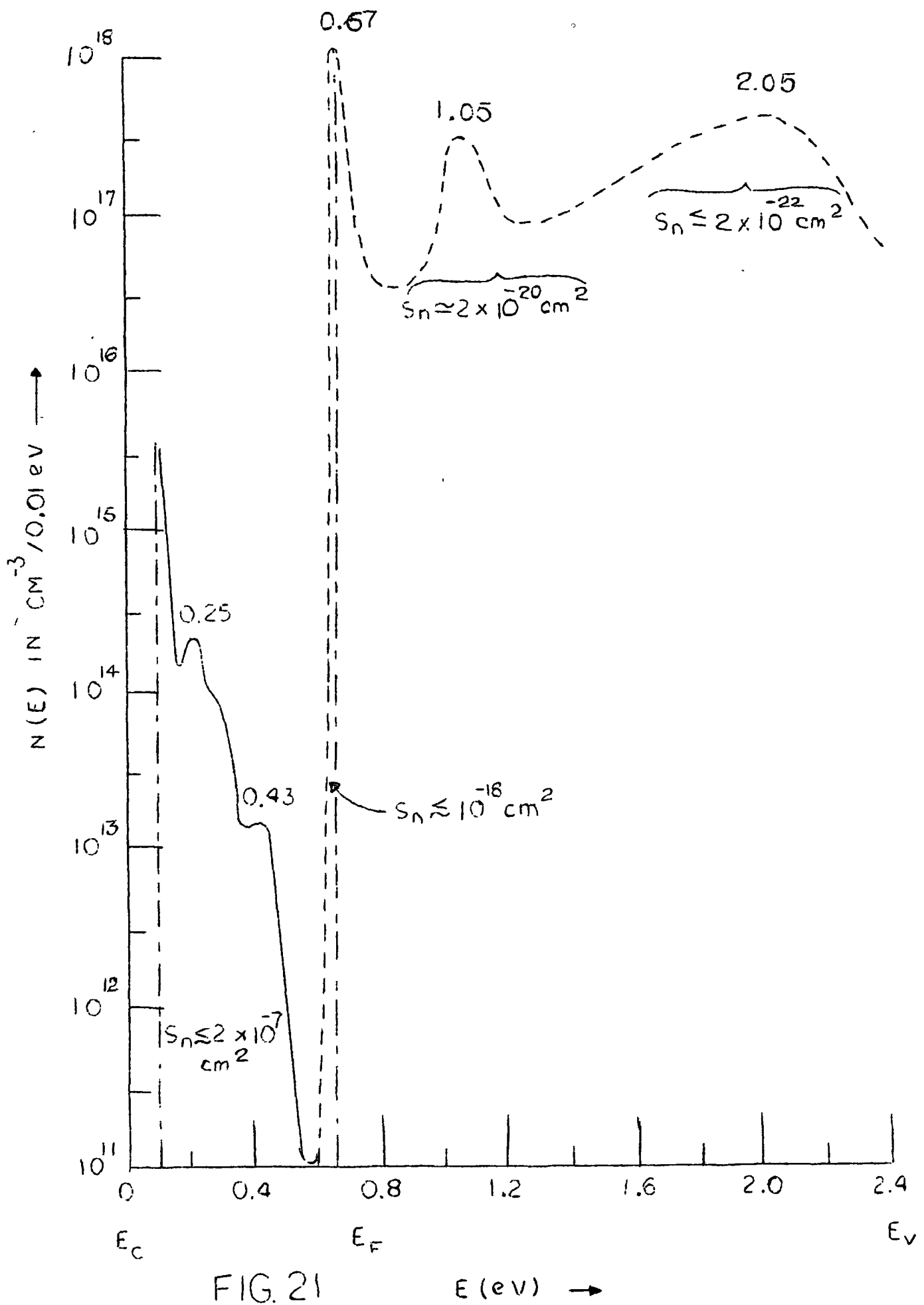
FIG. 21

DOCUMENT CONTROL DATA - R&D

(Security classification of title, body of abstract and indexing annotation must be entered when the overall report is classified)

1. ORIGINATING ACTIVITY *(Corporate author)*	2a. REPORT SECURITY CLASSIFICATION
K. W. Böer	2b. GROUP

3. REPORT TITLE

EVAPORATED AND RECRYSTALLIZED CdS LAYERS

4. DESCRIPTIVE NOTES *(Type of report and inclusive dates)*
Technical Report #11

5. AUTHOR(S) *(Last name, first name, initial)*

Böer, K. W., Esbitt, A. S., Kaufman, W. M.

6. REPORT DATE	7a. TOTAL NO. OF PAGES	7b. NO. OF REFS.
July, 1966	66	28

8a. CONTRACT OR GRANT NO.	9a. ORIGINATOR'S REPORT NUMBER(S)
(G) 4336 (00)	
b. PROJECT NO	#11
c	9b. OTHER REPORT NO(S) *(Any other numbers that may be assigned this report)*
d	

10. AVAILABILITY/LIMITATION NOTICES

None

11. SUPPLEMENTARY NOTES	12. SPONSORING MILITARY ACTIVITY
None	Navy

13. ABSTRACT

Heat treatments of evaporated CdS layers in nitrogen containing HCl and traces of oxygen, and providing a transport of CdS and copper are reported. Recrystallization of areas up to several mm^2 are observed. At $25^{\circ}C$, the treated layers show mobilities of 140 to 230 cm^2/Vs, photoconductivities of 10^{-3} to $2 \times 10^{-1} \Omega^{-1}cm^{-1}$ at 750 ft-c ($2600^{\circ}K$ white light) with light-to-dark-current ratios of $10^8 - 10^9$ and response time (decay) of 300 µs to 1.2 ms at 100 ft-c. The level distribution and capture cross section for electrons is investigated using spectral distribution, light intensity, and temperature dependence of photoconductivity, thermally stimulated current and response time analyses. Levels at 0.23, 0.43, 0.67, 1.05 and 2.05 eV are observed and the letter three attributed to Cu-centers. Compared to other layers and single crystals, these layers show a density of $<10^{12}$ cm^{-3} of levels attributed to sulfur vacancies in the range between 0.3 and 0.65 eV and a not detectable amount of intrinsic defects acting as quenching centers at 0.9 and 1.35 eV. This is explained by a Cu-enhanced recrystallization in a CdS-supplying atmosphere at temperatures (620° to $650^{\circ}C$) below the temperatures otherwise used for crystal growth, and thereby efficient annealing of intrinsic defects.

KEY WORDS	LINK A		LINK B		LINK C	
	ROLE	WT	ROLE	WT	ROLE	WT
CdS evaporated layers photoconductor recrystallization high mobility fast response time						

INSTRUCTIONS

1. ORIGINATING ACTIVITY: Enter the name and address of the contractor, subcontractor, grantee, Department of Defense activity or other organization (corporate author) issuing the report.

2a. REPORT SECURITY CLASSIFICATION: Enter the overall security classification of the report. Indicate whether "Restricted Data" is included. Marking is to be in accordance with appropriate security regulations.

2b. GROUP: Automatic downgrading is specified in DoD Directive 5200.10 and Armed Forces Industrial Manual. Enter the group number. Also, when applicable, show that optional markings have been used for Group 3 and Group 4 as authorized.

3. REPORT TITLE: Enter the complete report title in all capital letters. Titles in all cases should be unclassified. If a meaningful title cannot be selected without classification, show title classification in all capitals in parenthesis immediately following the title.

4. DESCRIPTIVE NOTES: If appropriate, enter the type of report, e.g., interim, progress, summary, annual, or final. Give the inclusive dates when a specific reporting period is covered.

5. AUTHOR(S): Enter the name(s) of author(s) as shown on or in the report. Enter last name, first name, middle initial. If military, show rank and branch of service. The name of the principal author is an absolute minimum requirement.

6. REPORT DATE: Enter the date of the report as day, month, year, or month, year. If more than one date appears on the report, use date of publication.

7a. TOTAL NUMBER OF PAGES: The total page count should follow normal pagination procedures, i.e., enter the number of pages containing information.

7b. NUMBER OF REFERENCES: Enter the total number of references cited in the report.

8a. CONTRACT OR GRANT NUMBER: If appropriate, enter the applicable number of the contract or grant under which the report was written.

8b, 8c, & 8d. PROJECT NUMBER: Enter the appropriate military department identification, such as project number, subproject number, system numbers, task number, etc.

9a. ORIGINATOR'S REPORT NUMBER(S): Enter the official report number by which the document will be identified and controlled by the originating activity. This number must be unique to this report.

9b. OTHER REPORT NUMBER(S): If the report has been assigned any other report numbers (either by the originator or by the sponsor), also enter this number(s).

10. AVAILABILITY/LIMITATION NOTICES: Enter any limitations on further dissemination of the report, other than those imposed by security classification, using standard statements such as:

(1) "Qualified requesters may obtain copies of this report from DDC."

(2) "Foreign announcement and dissemination of this report by DDC is not authorized."

(3) "U. S. Government agencies may obtain copies of this report directly from DDC. Other qualified DDC users shall request through

_____."

(4) "U. S. military agencies may obtain copies of this report directly from DDC. Other qualified users shall request through

_____."

(5) "All distribution of this report is controlled. Qualified DDC users shall request through

_____."

If the report has been furnished to the Office of Technical Services, Department of Commerce, for sale to the public, indicate this fact and enter the price, if known.

11. SUPPLEMENTARY NOTES: Use for additional explanatory notes.

12. SPONSORING MILITARY ACTIVITY: Enter the name of the departmental project office or laboratory sponsoring (paying for) the research and development. Include address.

13. ABSTRACT: Enter an abstract giving a brief and factual summary of the document indicative of the report, even though it may also appear elsewhere in the body of the technical report. If additional space is required, a continuation sheet shall be attached.

It is highly desirable that the abstract of classified reports be unclassified. Each paragraph of the abstract shall end with an indication of the military security classification of the information in the paragraph, represented as (TS), (S), (C), or (U).

There is no limitation on the length of the abstract. However, the suggested length is from 150 to 225 words.

14. KEY WORDS: Key words are technically meaningful terms or short phrases that characterize a report and may be used as index entries for cataloging the report. Key words must be selected so that no security classification is required. Identifiers, such as equipment model designation, trade name, military project code name, geographic location, may be used as key words but will be followed by an indication of technical context. The assignment of links, roles, and weights is optional.

DD FORM 1473 (BACK)

2N 66 74831